SIGMA RESEARCH, INC.
RICHLAND, WASHINGTON 99352

Heat Pipe Temperature Control Utilizing A Soluble Gas Absorption Reservoir

NASA CR-137,792

February 1976

by E. W. Saaski
Manager, Thermal Systems
Sigma Research, Inc.
2952 George Washington Way
Richland, Washington 99352

Prepared for
Ames Research Center
National Aeronautics and Space Administration
Moffet Field, California 94035

This document is the final report submitted by Sigma Research, Inc., Richland, Washington, for the program entitled "Heat Pipe Temperature Control Utilizing a Soluble Gas Absorption Reservoir" (NASA Order No. A 13415B). C. McCreight and M. Groll were the NASA Technical Managers.

This report covers the period 12 May 1975 through 7 November 1975.

NASA CR 137,792

HEAT PIPE TEMPERATURE CONTROL UTILIZING A SOLUBLE GAS ABSORPTION RESERVOIR

by

E. W. Saaski

February 1976

Sigma Research, Inc.
2952 George Washington Way
Richland, Washington 99352

for

AMES RESEARCH CENTER
NATIONAL AERONAUTICS AND SPACE ADMINISTRATION
MOFFETT FIELD, CALIFORNIA 94035

ABSTRACT

A new gas-controlled heat pipe design is described which uses a liquid matrix reservoir, or sponge, to replace the standard gas reservoir. Reservoir volume may be reduced by a factor of five to ten for certain gas-liquid combinations, while retaining the same level of temperature control. Experiments with ammonia, butane, and carbon dioxide control gases with methanol working fluid are discussed.

CONTENTS

SYMBOL TABLE

A_c = condenser cross-section, cm^2

A_ℓ = reservoir wick vapor contact area, cm^2

A_w = cross-sectional area of heat pipe wall, cm^2

C, $C_{g\ell}$ = liquid phase noncondensable gas concentration, g-moles/cm^3

C_{gv} = vapor phase noncondensable gas concentration, g-moles/cm^3

C_o = pretransient dissolved gas concentration, moles/cm^3

D_{ab} = gas diffusivity in liquid, cm^2/sec

G_c = per-unit-length condenser conductance, W/cmK

G_f = conductance of fin defined by gas leg ℓ_g, W/cmK

K_w = thermal conductivity of heat pipe wall, W/cmK

ℓ = reservoir wick thickness, cm

ℓ_c = condenser length, cm

ℓ_g = gas leg length, cm

mC_p = heat pipe thermal mass, joules/K

N_o = total moles of noncondensable gas, g-moles

P_s = saturation vapor pressure, atm.

Q = heat transfer rate, watts

r_a = artery radius, cm

$r_{1,2}$ = principal radii of curvature, cm

t = time, sec

T_c = critical temperature, K

T_s = sink temperature, K

T_v = vapor temperature - assumed independent of position in evaporator or adiabatic, K

V_r = reservoir volume, cm^3

$V_{\ell r}$ = liquid-vapor matrix total volume, cm^3

α = Ostwald coefficient

β_c = fraction of condenser filled with wick/fluid composite

β_r = fraction of reservoir filled with wick/fluid composite

γ = surface tension, dynes/cm

δ = gap width, cm

η_c = fraction of wick/fluid composite filled with fluid in condenser

η_r = fraction of wick/fluid composite filled with fluid in reservoir

θ_c = See equation 6

θ_r = See equation 6

θ_r^+ = See equation 19

τ_D = diffusive time constant, sec

τ_{th} = thermal time constant, sec

$\langle C \rangle$ = average value of C

FIGURES

TABLES

1.0 INTRODUCTION

This report describes analysis and experiments for a new type of thermal control device called a gas absorption reservoir heat pipe. Briefly, the device maintains a relatively stable heat source temperature by a stagnant gas leg in the condenser which moves in response to varying heat input, as occurs with a gas-controlled heat pipe. The device differs from the standard gas controlled heat pipe in that the gas reservoir associated with the heat pipe is replaced by a much smaller liquid reservoir. For a number of gas/fluid combinations, it can be shown that it is volumetrically more efficient to store gas as a dissolved solute than dispersed as a gas in a vapor reservoir. In the experiments described in this report, temperature stability has been improved by a factor of 2.5 or more over a gas reservoir of equal volume with the gases ammonia and butane in methanol. For the heat pipe tested, equivalent temperature control would have required a gas reservoir over 5 times the volume of the liquid sponge reservoir.

The absorption reservoir heat pipe has some drawbacks, however, including potentially longer response times to step-changes in heat transfer rate. Section 2, Analysis, discusses absorption reservoir design in some detail. Section 3, Experimental Tests, describes experimental methods, presents experimental data, and correlates the data with models presented in Section 2. Section 4 summarizes the analytical and experimental program, and suggests future development work in this area.

2.0 ANALYSIS

The first section presents basic equations describing the steady-state response of a gas-absorption reservoir heat pipe and compares the derived equations with those for a gas-controlled heat pipe embodying a gas reservoir. The next section discusses possible gas-liquid combinations for room-temperature and cryogenic operation found from a literature search. The third and last section addresses the effect of rapid source strength variations, which may temporarily drive the gas absorption reservoir heat pipe to higher than equilibrium operating temperatures because of a rate-limiting process of gas diffusion into the liquid reservoir.

2.1 Basic Operating Theory

Figure 2.1 presents a comparison between the standard gas-controlled heat pipe and the gas absorption reservoir heat pipe. The standard design comprises a condenser active length ℓ_c and a gas reservoir of volume V_r. The equivalent gas absorption reservoir heat pipe has a liquid storage volume storing $V_{\ell R}$ volume of fluid and gas, but is otherwise identical to the first heat pipe. Each has a total cross-sectional area A_c in the condenser, which is independent of axial position.

If for purposes of comparison the gas front is assumed sharp (i.e., a flat front), then simple closed-form models of the two systems are possible. For thermal comparison, assume it is necessary to design a gas-controlled heat pipe with the following constraints:

1. At vapor core temperature T_1, the gas front shall be at $\ell_g = \ell_c$.
2. At vapor core temperature T_2, the gas front shall be at $\ell_g = 0$.
3. The sink temperature is T_0, and the gas zone can be assumed to also be at T_0.

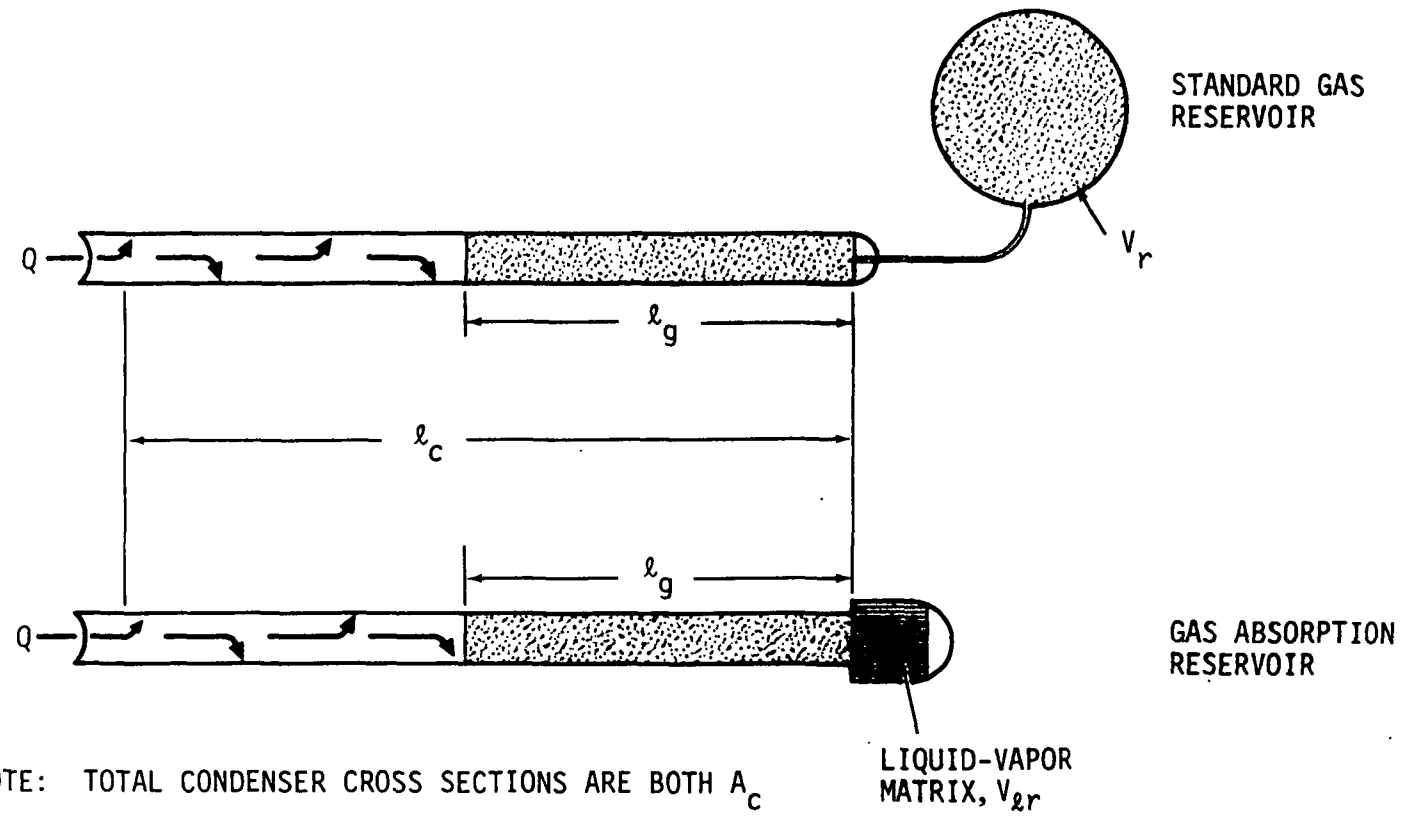

NOTE: TOTAL CONDENSER CROSS SECTIONS ARE BOTH A_c

FIGURE 2.1 A COMPARISON OF GAS RESERVOIR AND GAS ABSORPTION RESERVOIR HEAT PIPE CONDENSER ASSEMBLIES

4. The gas reservoir temperature is at T_0, and the reservoir is wicked.

5. Ambient temperature is constant.

The wicked reservoir heat pipe described above operates nominally at $0.5\ (T_1 + T_2)$ with control range $\pm 0.5\ (T_2 - T_1)$. By invoking conservation of noncondensable gas (NCG) at constraints (1) and (2), the NCG reservoir can be sized in terms of other thermophysical characteristics:

$$V_r = \frac{\left(P_{S1} - P_{S0}\right)}{\left(P_{S2} - P_{S1}\right)} \cdot A_c \ell_c \, (1-\beta_c)/(1-\beta_r) \qquad (1)$$

where P_{Si} corresponds to the saturation vapor pressure at temperature T_i, and β_c and β_r are the fractions of condenser and reservoir volumes respectively filled with wick and fluid.

If the gas reservoir is replaced by a liquid-vapor matrix with total volume $V_{\ell r}$ and liquid volume $\eta_r \beta_r V_{\ell r}$, then under conditions of vapor-liquid equilibrium, the concentrations of NCG in the two phases will be related by

$$C_{g\ell} = \alpha C_{gv} \qquad (\text{g-moles/cm}^3) \qquad (2)$$

where $C_{g\ell}$ is the molar gas density in the liquid phase and C_{gv} is the molar gas density in the vapor phase. The factor α is the Ostwald coefficient and is a constant for dilute solutions, although it may be dependent on concentration at high concentration and/or high gas partial pressure. The fraction of reservoir volume filled with fluid is $\eta_r \beta_r$; η_r is the fluid volume fraction of the reservoir wick/fluid composite. The fractional fluid fill in the condenser wick/fluid composite is correspondingly given by η_c. If conservation of NCG is invoked at conditions (1) and (2), the following is obtained:

$$N_o = C_{gv}(T_1)\left[A_c \ell_c \theta_c + V_{\ell r}\theta_r\right] \quad \text{(Condition 1)} \qquad (3)$$

$$N_o = C_{gv}(T_2)\theta_r V_{\ell r} \quad \text{(Condition 2)} \qquad (4)$$

where

$$C_{gv}(T_i) = \frac{P_{Si} - P_{SO}}{RT_o} \qquad (5)$$

and

$$\theta_c = 1 + \beta_c(\alpha\eta_c - 1); \quad \theta_r = 1 + \beta_r(\alpha\eta_r - 1) \qquad (6)$$

If expressions (3) and (4) are set equal to each other and $V_{\ell r}$ is solved for, it is found that

$$V_{\ell r} = \frac{(P_{S1} - P_{SO})}{(P_{S2} - P_{S1})} \cdot A_c \ell_c \cdot \frac{\theta_c}{\theta_r} \qquad (7)$$

If, for purposes of comparison, it is assumed in equation (7) that η_r is very close to 1.0 and β_c is much less than 1.0, then it is clear that expressions (1) and (7) differ by only the multiplicative constant $1/\alpha\beta_r$ if β_c and β_r are both small in equation (1) and α is much larger than one. That is, the required liquid reservoir volume for a given amount of temperature control is on the order of $1/\alpha\beta_r$ times the gaseous volume needed in a typical gas reservoir heat pipe.

Phrased another way, if gas/fluid combinations can be found where α is significantly greater than 1.0 and $\eta_c\beta_c$ is small, then it is volumetrically more efficient to store the gas as a dissolved solute than dispersed in a vapor phase reservoir. Such combinations are possible but common control gases do not satisfy this criteria.

2.2 Candidate Gas/Fluid Systems

As discussed in Section 2.1, it is volumetrically more efficient to store a noncondensable gas in the form of a dissolved solute than to store the gas dispersed in a vapor phase if the Ostwald coefficient is greater than 1. It is thus desirable to use systems with the highest Ostwald coefficient possible for gas absorption heat pipes, unless very high solubility contributes to deleterious side effects.

Stable heat pipe operation has been previously demonstrated for α in the range 20 to 30. In Reference 1, Saaski operated both Cl_2/CCl_4 and $Cl_2/CFCl_3$ systems in the reflux mode for temperatures between 10^o and 100^oC with satisfactory component separation. Ostwald coefficients as a function of temperature are shown in Figure 2.2. Both carbon tetrachloride and R-11 are unfortunately rather poor heat pipe fluids, and a literature search was accomplished to determine if there existed more optimum fluid/gas combinations.

Table 2.1 presents Ostwald coefficient data from Reference 2 for a large number of gas/liquid combinations at 25^oC. The common control gases such as He, N_2 and Ar are seen to have Ostwald coefficients strictly less than 1, and are unsatisfactory. Large molecules such as Kr, CO_2, Xe and C_2H_6 do have Ostwald coefficients greater than 1, but the largest value is on the order of 5. This is somewhat marginal. To demonstrate a significant advantage over present gas reservoir designs, it would be desirable to use a gas/fluid combination with an Ostwald coefficient of 10 to 20. As discussed in Section 2.3, some void volume must be left in the reservoir for optimum reservoir response, and a fluid/wick volume fraction β_R of 0.5 is a realistic goal. Reservoir size reduction would therefore be on the order of 1/5 to 1/10.

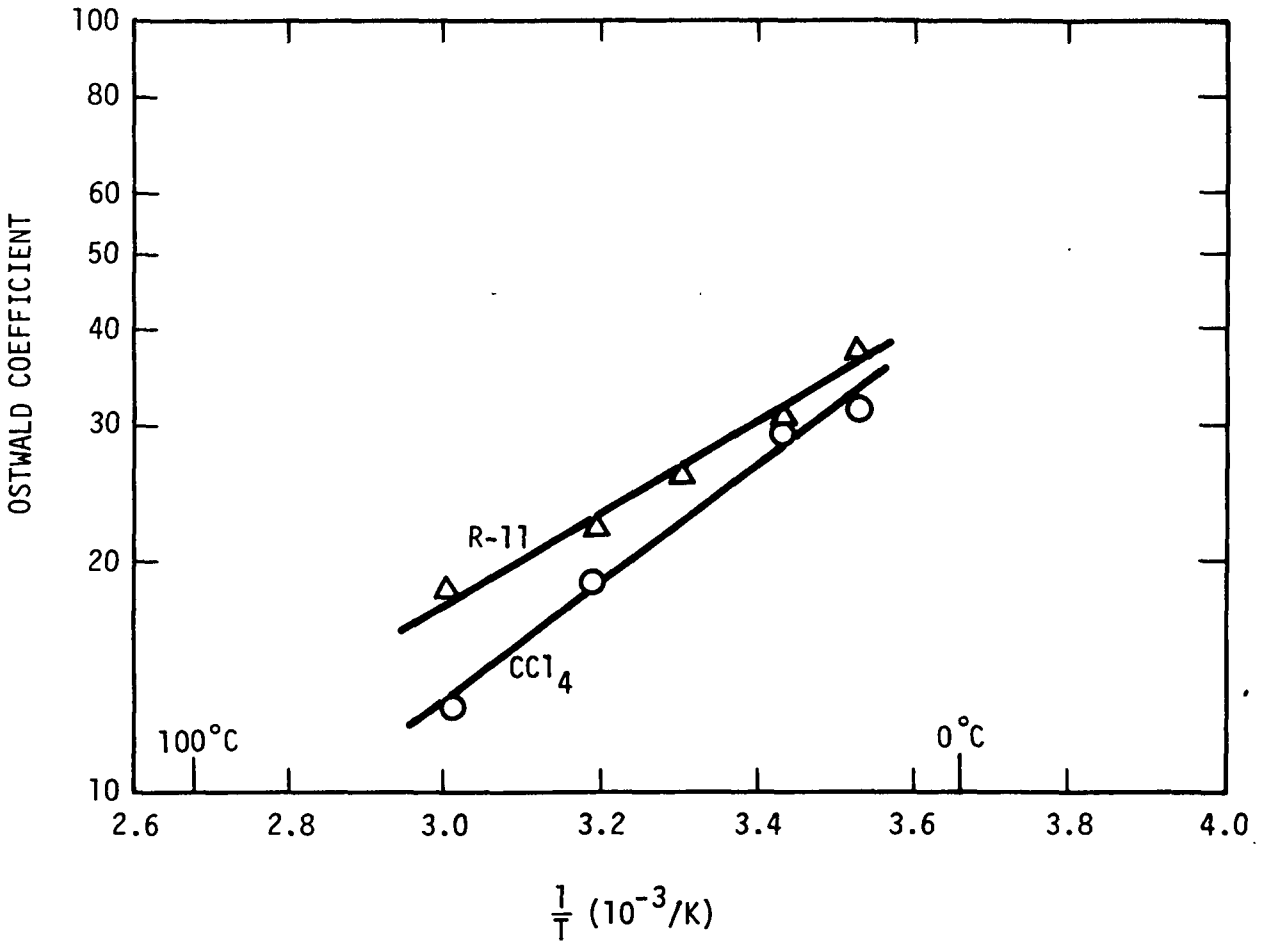

FIGURE 2.2 THE SOLUBILITY OF CHLORINE IN CCl_4 AND R-11 ($CFCl_3$)

TABLE 2.1. EXPERIMENTAL OSTWALD COEFFICIENTS AT 25°C FOR A NUMBER OF GASES AND FLUIDS

Liquid	He	Ne	H_2	N_2	Co	O_2	Ar	CH_4	Kr	CF_4	CO_2	Xe	C_2H_6	Rn	C_2F_6
Freon-113	--	0.099	0.134	--	--	--	0.6200	--	--	0.978		4.3900	5.8300	--	3.05
Ethyl ether	--	--	0.1300	0.2950	0.3980	0.4660	--	1.0670	--		5.3700	--	--	14.000	--
Freon-21	0.0525	--	--	--	--	--	0.5130	--	--		--	--	--	--	--
Cyclohexane	0.0275	0.0419	0.0860	0.1740	--	--	0.3330	0.6630	1.0550	0.233	1.7100	4.5000	--	--	--
CCl_4	--	--	0.0828	0.1630	0.2240	0.3040	0.3400	0.7240	--	0.301	2.7000	--	5.2700	--	--
Benzene	0.0210	0.0315	0.0710	0.1230	0.1640	0.2240	0.2400	0.5700	0.7510	0.157	2.6700	3.0800	4.0700	--	0.3040
Acetone	0.0362	0.0520	0.0769	0.1970	0.2540	0.3080	0.3010	0.7420	--		6.9800	--	--	5.800	--
Chloroform	--	--	0.0672	0.1360	0.1970	0.2250	--	--	--		3.7000	--	--	13.800	--
Chlorobenzene	--	--	0.0640	0.1030	0.1520	0.1900	--	0.5000			2.3600	--	3.5500	--	--
Ethanol	0.0319	0.0455	0.0890	0.1420	0.1930	0.1560	0.2580	--	--		3.2700	--	2.7500	5.700	--
Ammonia	0.0316	--	0.0722	0.0895	--	--	0.1460	--	--		--	--	--	--	--
Glycol	--	--	--	0.0153	--	--	0.0370	--	--		--	--	0.2350	--	--
Methanol	0.0360	0.0486	0.0947	0.1420	0.1960	0.1920	0.2680	0.4280	--		--	--	2.3400	--	--
Water	0.0097	0.0111	0.0190	0.0156	--	0.0310	0.0343	0.0329	0.0610		0.8300	0.1220	0.0450	0.2240	--
Sodium[1]	$3.34(10^{-4})$			$3.11(10^{-8})$			$2.27(10^{-5})$		$3.57(10^{-6})$			0.2730			

(1) at 500°C

Table 2.2 presents Ostwald coefficients for several room temperature combinations. It can be seen that several gas/liquid combinations are available for laboratory ambient heat pipes, and system solubilities are in a useful range. In some cases binary combinations such as water-methanol could be more appropriately classified as two-fluid media because of an extremely high mutual solutility. In these situations, the Ostwald coefficient is not quantitatively useful because the solubility is dependent on both pressure and temperature, and dissolution of large amounts of solute leads to nonideal behavior.

Methanol was selected as a working fluid for room temperature tests. In addition to being widely used as a heat pipe working fluid, a relatively low vapor pressure minimizes gravity-stratification of the condenser gas front. Non-perpendicular gas fronts have been observed in high-pressure ammonia-xenon heat pipes during 1-g tests, and this behavior has been observed to create erratic response. By using a low pressure (corresponding low density) working fluid having relatively low molecular weight, stratification with control gases of dissimilar molecular weight is minimized. Figure 2.3 shows experimental data from Reference 5 on the solution of various gases in methanol as a function of temperature. In all cases, the gas partial pressure is 1.0 atmosphere. In experiments discussed in Section 3, the gases nitrogen, carbon dioxide, butane, and ammonia were used. Ammonia is not presented in Figure 2.3, but the solubility is estimated to be higher than SO_2. In all cases, the solubility is approximately exponential in temperature.

This exponential behavior is also found for highly soluble gases in cryogenic working fluids. Figures 2.4 and 2.5 show data for several cryogenic combinations. References for these combinations are given in Table 2.3.

TABLE 2.2 ROOM TEMPERATURE GAS-LIQUID COMBINATIONS HAVING HIGH SOLUBILITY

Solvent	Solute	Temperature (°C)	Ostwald Coefficient	Ref.
Hexane	n-Propane	25	23.6	(3)
Benzene	n-Propane	25	16.0	(3)
Benzene	n-Pentane	16	312.0	(4)
Menthanol	Propane	25	3.4	(5)
Menthanol	Carbon Dioxide	12	4.1	(5)
Menthanol	Butane	12	28.0	(5)
Menthanol	Sulfur Dioxide	25	83.0	(5)
Menthanol	Carbon Dioxide	59	39.0	(6)
Water	Ammonia	25	40.7	(5)
Water	Sulfur Dioxide	25	34.0	(5)
Water	Menthanol	100	254.0	(7)

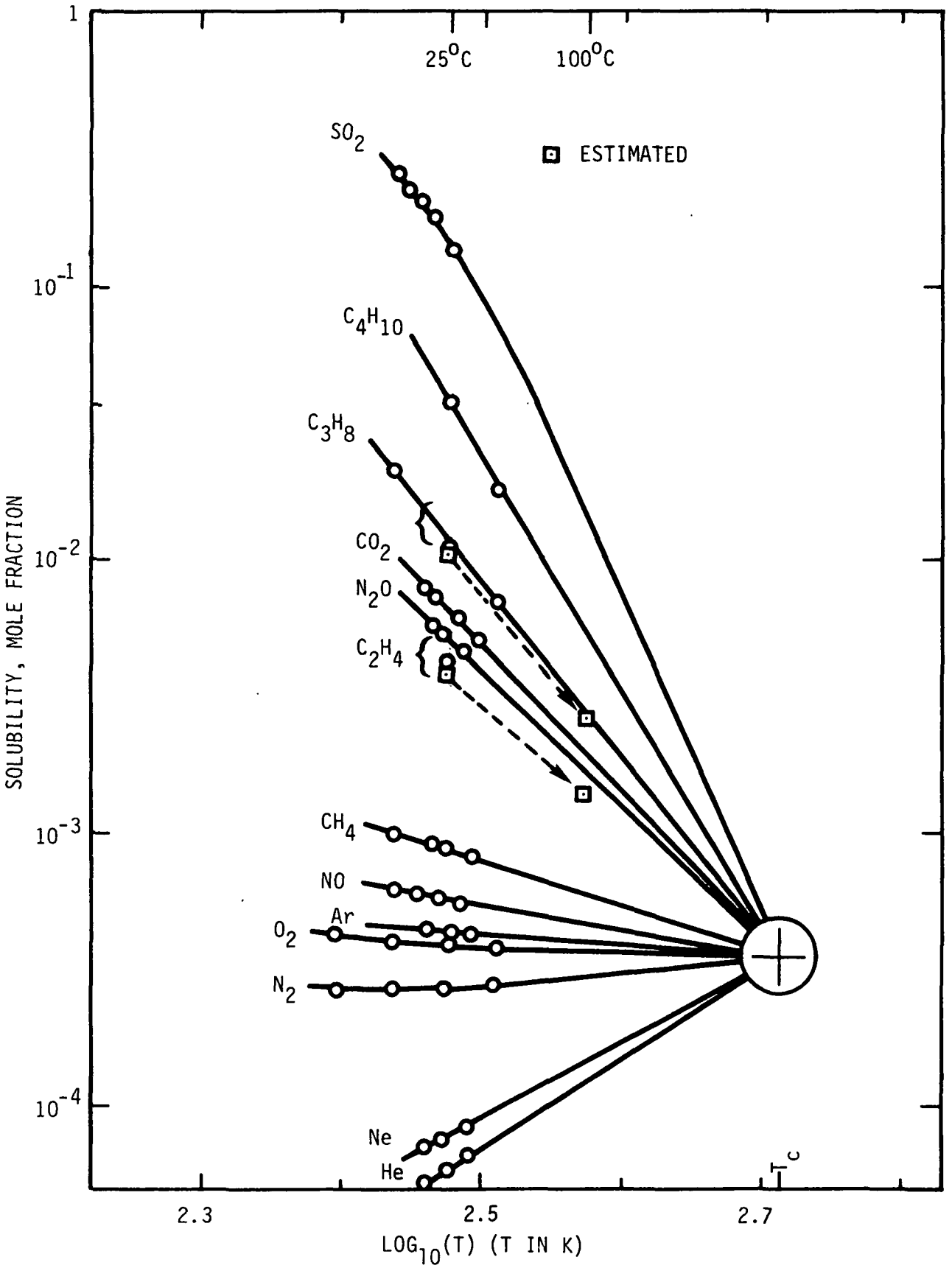

FIGURE 2.3 SOLUBILITY OF VARIOUS GASES IN METHANOL AS A FUNCTION OF TEMPERATURE (FROM REFERENCE 5)

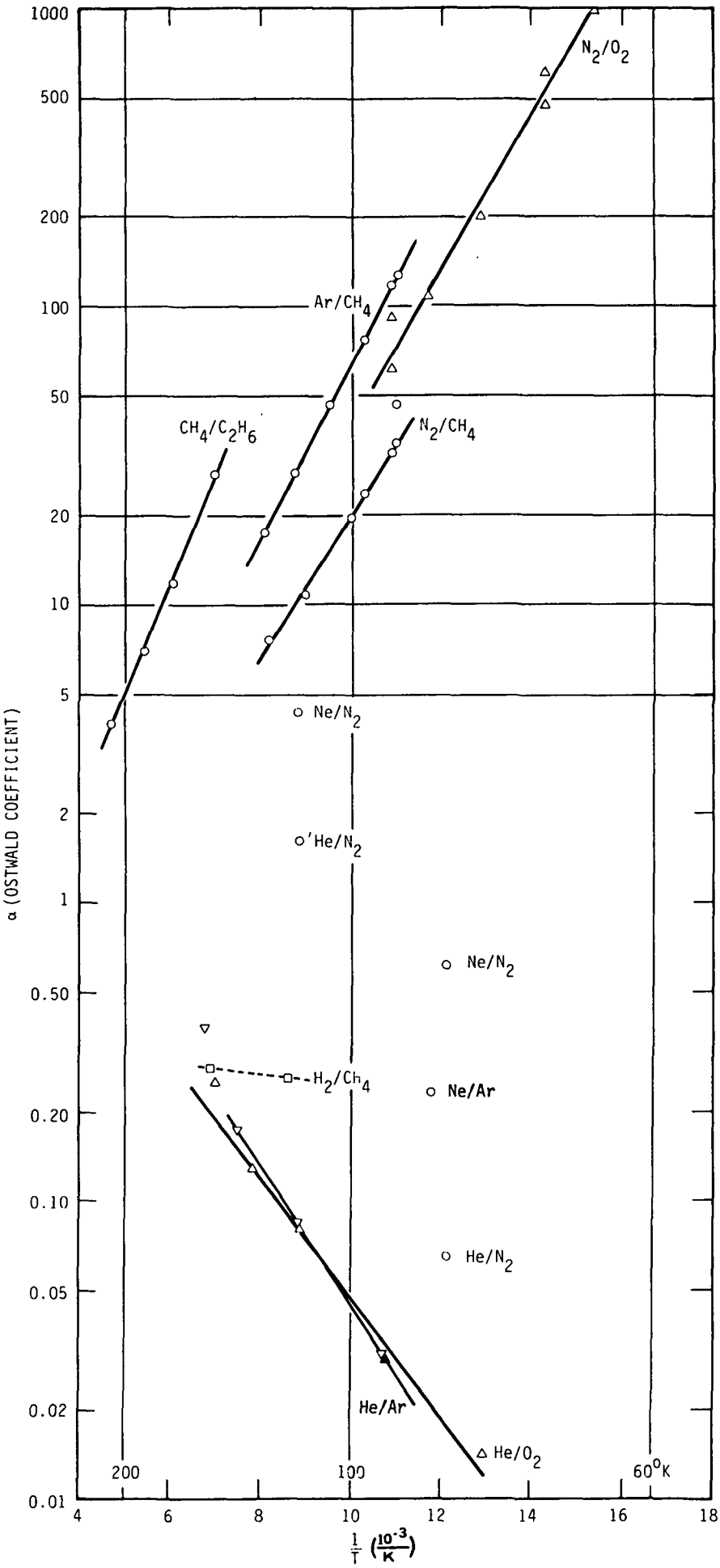

FIGURE 2.4 OSTWALD COEFFICIENT FOR SEVERAL CRYOGENIC BINARY GAS/LIQUID SYSTEMS

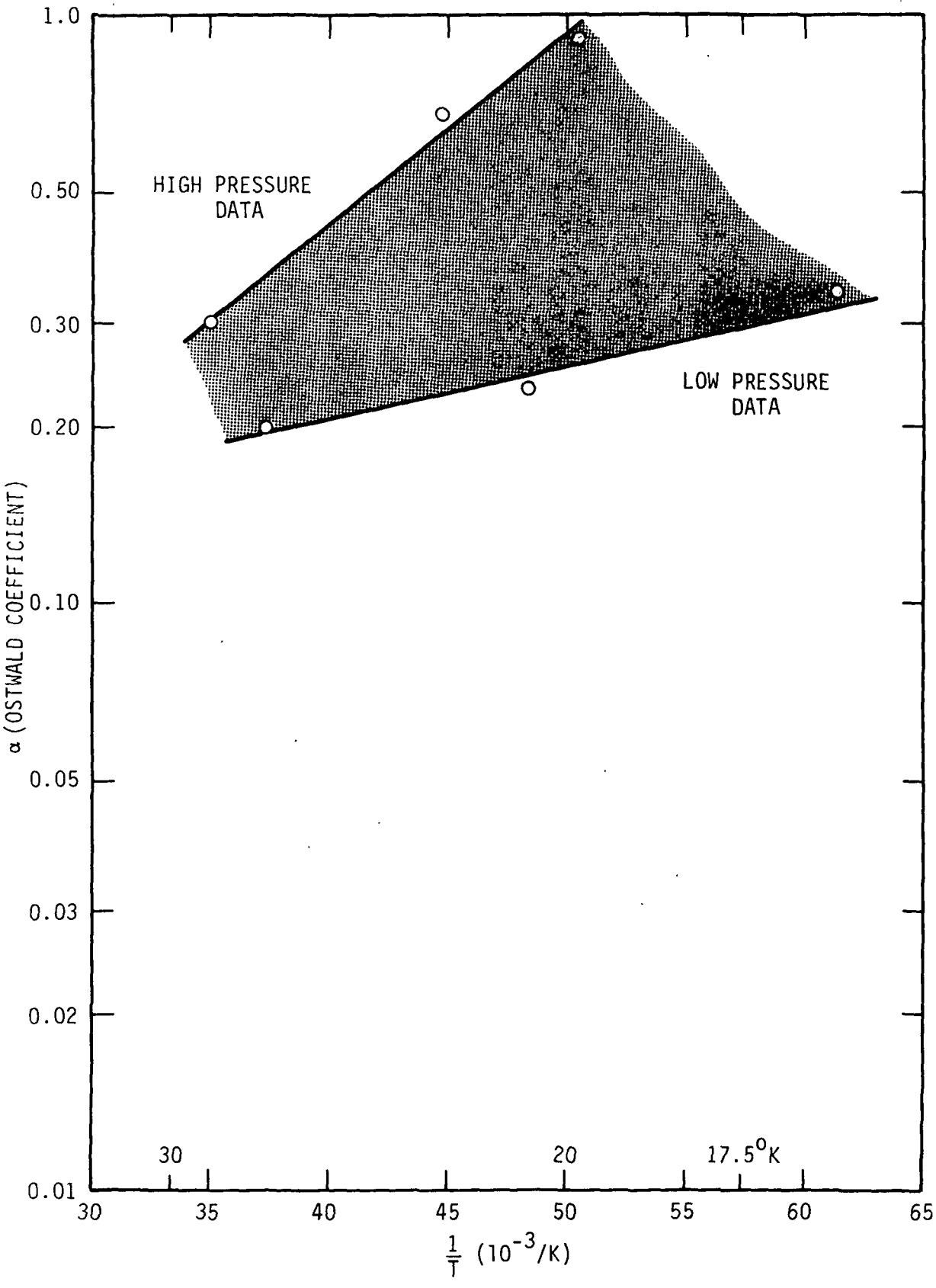

FIGURE 2.5 THE SOLUBILITY OF HELIUM IN LIQUID n-HYDROGEN FOR PARTIAL PRESSURES OF HELIUM BETWEEN 1.7 AND 7.6 ATMOSPHERES

TABLE 2.3. REFERENCES FOR CRYOGENIC BINARY GAS/LIQUID SOLUBILITY DATA

Gas/Fluid System	Reference Numbers
He/H_2	8
He/Ar	9, 10
He/N_2	11
He/O_2	10
H_2/CH_4	12
Ne/Ar	9
Ne/N_2	11
N_2/O_2	13, 14
N_2/CH_4	15, 16
Ar/CH_4	15, 16
CH_4/C_2H_6	7

Table 2.4 gives fitting constants A and B for cryogenic combinations of interest where the Ostwald coefficient is modeled as

$$\alpha \cong A \quad EXP(+B/T) \tag{8}$$

and where T is the system temperature in degrees Kelvin. The exponential coefficient B ranges from 550 to 1850 K and the pre-exponential factor is between 0.07 and 0.10. Systems of potential interest include

1. methane/ethane
2. argon/methane
3. nitrogen/methane
4. nitrogen/oxygen

The solubility of helium in hydrogen is surprisingly low as shown in Figure 2.5 and, hence, this technique would not be practical for liquid hydrogen nor, of course, helium.

The general exponential dependence of solubility on temperature is of both beneficial and adverse effect. Because of the rapid solubility decrease with temperature, condensate originating near the cold gas front becomes supersaturated as the fluid warms in transit to the evaporator, and gas stripping is augmented. This serves to maintain a sharp gas front. Conversely, the sensitivity to temperature can create problems in set-point maintenance. If liquid reservoir temperature is not maintained constant, the amount of dissolved gas in the liquid will fluctuate in response to temperature variations. The most direct consequence of this will be a fluctuation in both gas front position and heat pipe operating temperature. This sensitivity to reservoir temperature is also found in the wicked reservoir heat pipe where the reservoir working fluid partial pressure is exponentially dependent on reservoir temperature.

TABLE 2.4. CURVE-FITTING CONSTANTS FOR BINARY CRYOGENIC SYSTEMS SHOWING EXPONENTIAL SOLUBILITY BEHAVIOR

Gas/Liquid System	A	B (K)
CH_4/C_2H_6	0.0713	848
Ar/CH_4	0.0748	673
N_2/CH_4	0.0821	549
N_2/O_2	0.100	599

2.3 Transient Response-Reservoir Design

Two criteria dominate the physical design of an absorption reservoir. First, there must be adequate contact between the absorbing liquid and the vapor phase to ensure speedy equilibration of dissolved gas content in response to changes in thermal input because of typically low solute diffusion rates in liquid. Second, the vapor spaces used for vapor communication cannot be so small that they prime and drain liquid away from working sections of the heat pipe. In addition, complete filling of the reservoir with liquid will result in slow transient response.

In a representative reservoir design, the liquid would be contained in a very porous sheet of capillary material wrapped in a spiral so that the principal fluid priming radii of curvature for the inter-spiral gas gaps would sum to a constant.

$$\Delta P_\delta = \gamma\left[\frac{1}{r_1} + \frac{1}{r_2}\right] \tag{9}$$

where r_1 and r_2 are principal radii of curvature for the gap, and γ is surface tension.

For a spiral of constant pitch and inter-spiral gap width δ, this pumping pressure is approximately

$$\Delta P_\delta \cong \frac{2\gamma}{\delta} \tag{10}$$

If it is necessary to prime a capillary structure such as an artery of radius r_a, then to ensure proper priming of the artery it must be true that

$$\frac{2\gamma}{r_a} > \frac{2\gamma}{\delta} \tag{11}$$

If the heat pipe is tested in 1-g then the effects of gravity must also be included.

Equation 11 presents a criterion relating minimum size of reservoir gas gaps to characteristic capillary pumping structure dimensions in the heat pipe. To characterize maximum fluid absorber thickness, and thereby define the void/volume ratio in the reservoir, it is necessary to establish reservoir response to fluctuating heat inputs.

2.3.1 Reservoir Response-Slab Model

A representative concentration profile for a section of absorber is shown in Figure 2.6 after a step-decrease in power, i.e., a reduction in non-condensable gas partial pressure. If a unit cell of the absorber is modeled as a thin disc or slab, then the average time-dependent excess concentration is given as the series

$$\bar{C}^*(t) = \frac{8}{\pi^2} \sum_{N=0}^{\infty} \frac{EXP\left(-(2N+1)^2 D^* t\right)}{(2N+1)^2} \tag{12}$$

where $D^* = \left(\frac{\pi}{\ell}\right)^2 D_{ab}$

and D_{ab} is the binary gas/fluid diffusivity and ℓ is the overall thickness of a given disc. A derivation of this equation is given in Appendix A. The excess concentration $\bar{C}^*$ is defined as

$$\bar{C}^* = \frac{\langle C - C_o \rangle}{C_m - C_o} \tag{13}$$

where C_m is the pre-transient dissolved gas concentration and C_o is the post-transient equilibrium gas concentration. This dimensionless concentration is shown as a function of the grouping $D_{ab}t/\ell^2$ in Figure 2.7. For this grouping greater than 0.025, the dimensionless concentration is given approximately as

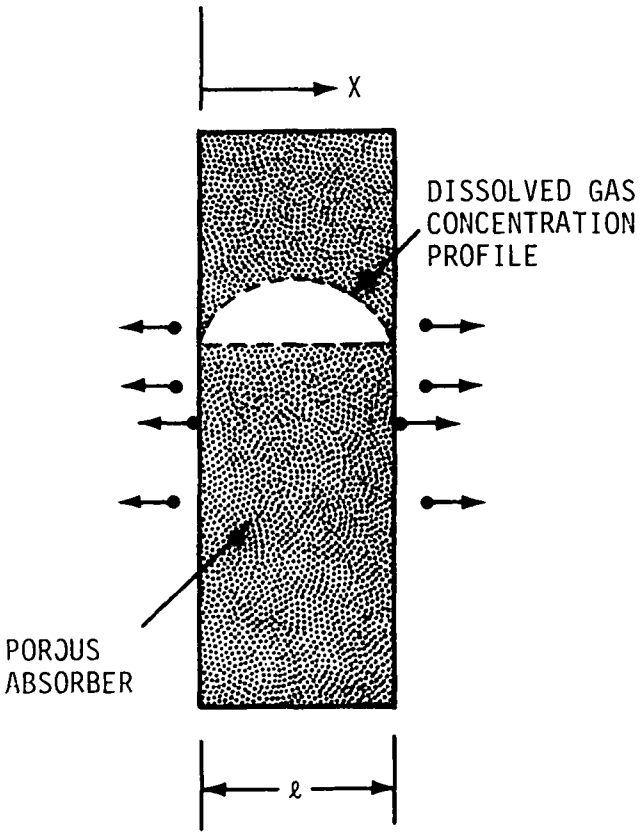

FIGURE 2.6 ONE-DIMENSIONAL SLAB MODEL OF ABSORPTION RESERVIOR UNIT CELL. WITH A STEP-CHANGE IN EXTERNAL GAS CONCENTRATION, THE POROUS LIQUID-SATURATED ABSORBER RE-ESTABLISHES EQUILIBRIUM BY GAS/LIQUID DIFFUSION.

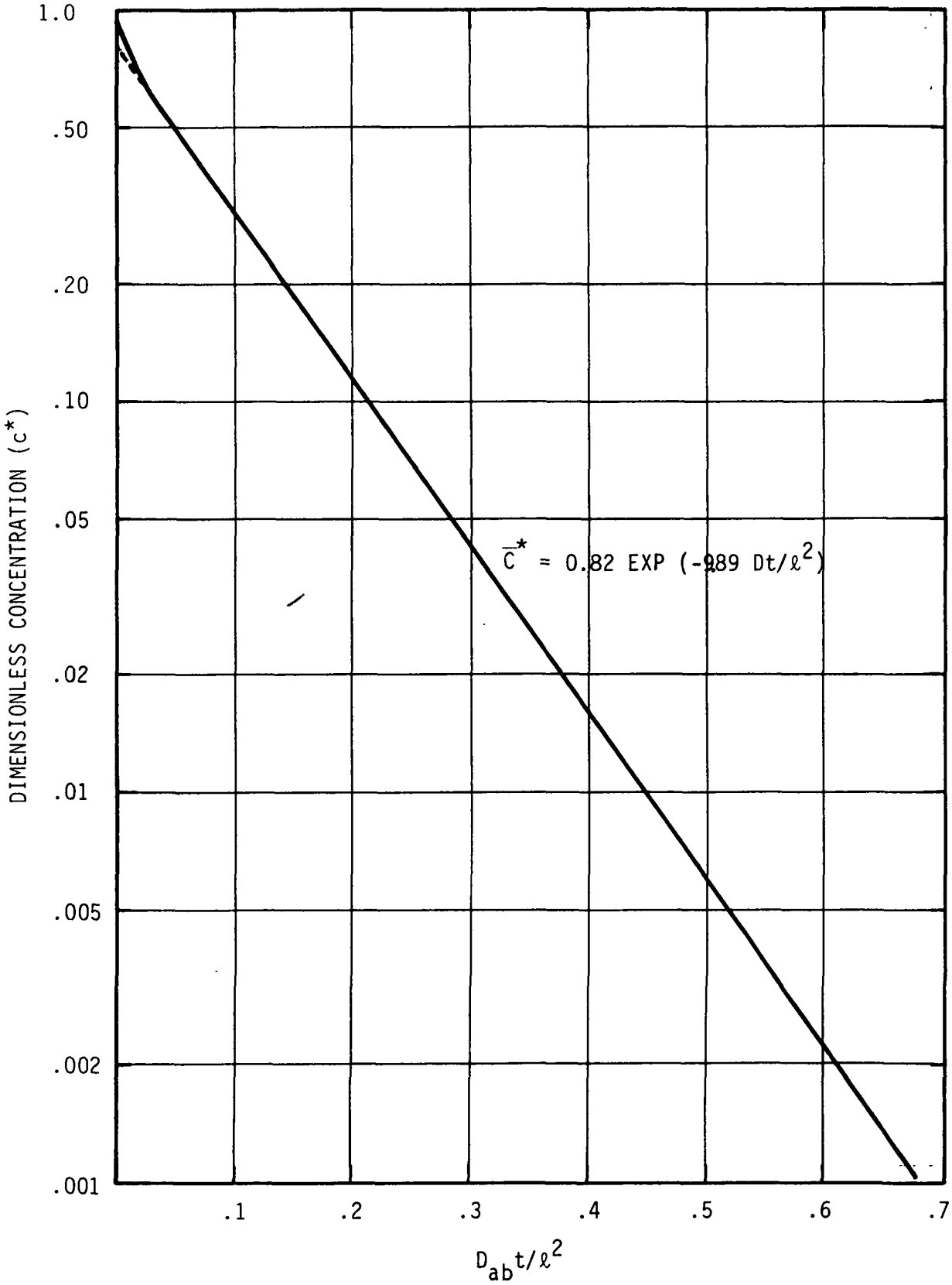

FIGURE 2.7 DIMENSIONLESS AVERAGE CONCENTRATION IN A SLAB AS A FUNCTION OF THE GROUPING $D_{ab}t/\ell^2$.

$$\bar{C}^* \cong 0.82 \text{ EXP } (-9.89\ Dt/\ell^2) \qquad (14)$$

At time equal zero, $\bar{C}^* \equiv 1.$, while at $t = \infty$, $\bar{C}^* \equiv 0$. At some finite time $\bar{C}^*$ is negligibly small. If $\bar{C}^* = 0.01$ is arbitrarily selected as negligibly small, then a characteristic time constant τ for diffusion-driven equilibrium is obtained

$$\tau = 0.446\ \ell^2/D_{ab} \qquad \text{(secs)} \qquad (15)$$

Because cryogenic heat pipe design is currently of high interest and fluid diffusivities can be expected to be low, values of τ have been calculated for several cryogenic fluids using the following expression for the diffusivity

$$D_{ab} = \frac{9.76(10^{-8})\ (M_b\psi)^{1/2}T}{\mu_b\sigma_a^{1.8}} \qquad (16)$$

where

D_{ab} = diffusion coefficient, a → b (cm^2/sec)

M_b = solvent molecular weight

ψ = association parameter (water = 2.6, methanol = 1.9, benzene = 1.0, etc.)

T = temperature (^oK)

μ_b = solvent viscosity (centipoise)

σ_a = molecular diameter, A^o

This is a modified form of the Wilke-Chang empirical diffusivity formula as given in Reference 2. Since this was derived from room temperature data, it was necessary to check the model against experimental cryogenic data. This was done for the data of Ricci (Ref. 17) for various gases in liquid nitrogen. Figure 2.8 shows correlation of Ricci's data with the empirical model (16) for the gases Ne, Ar, and CH_4. The temperature dependence of diffusivity is

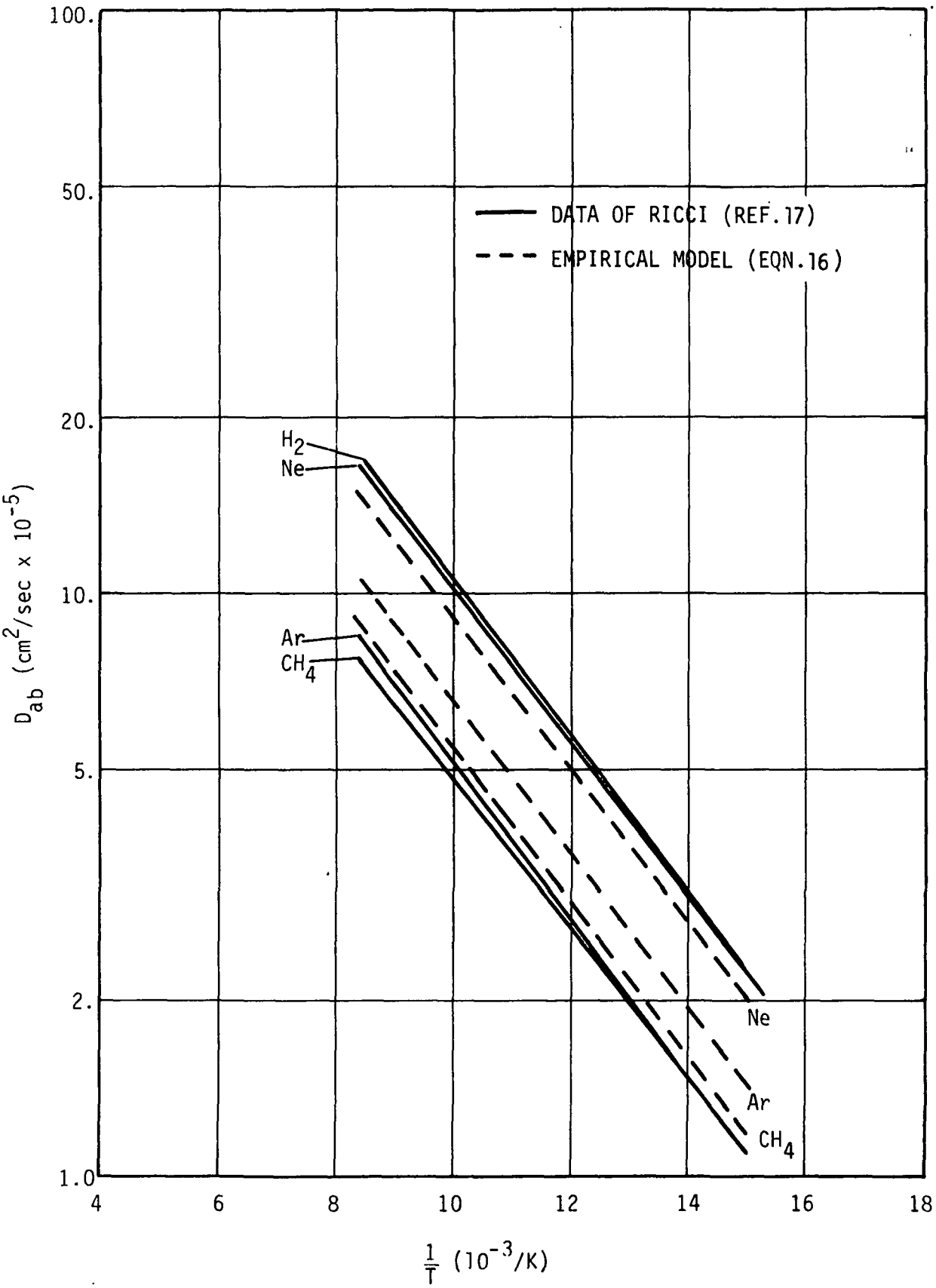

FIGURE 2.8 A COMPARISON OF THE DATA OF RICCI WITH THE WILKE-CHANG EMPIRICAL MODEL FOR GAS/LIQUID DIFFUSIVITY. LIQUID NITROGEN IS SOLVENT.

represented very well, although the absolute values differ by as much as 30%. However, this is adequate agreement for scoping purposes.

In the previous section, several cryogenic gas/liquid combinations were identified as of potential interest. These were

1. methane/ethane
2. argon/methane
3. nitrogen/methane
4. nitrogen/oxygen

With the model (16), the diffusivities shown in Figure 2.9 were calculated. The diffusivities are typically from 2×10^{-5} cm^2/sec to 10×10^{-5} cm^2/sec. Before using these values of D_{ab} to calculate τ, the values were multiplied by 0.40 to account for permeability of the porous slab used as a gas absorber. This correction factor was based on the experimental data of Saaski (Ref. 2) for double-thickness square-weave screens.

Characteristic time constants are presented in Table 2.5 for the fluids previously noted, using Equation 16 and a correction factor of 0.40 to D_{ab}. A slab thickness of 0.050 cm was selected as representative of absorber thickness: the time constant scales as ℓ^2 for other thicknesses. For this particular choice of ℓ, time constants of 0.6 to 2.3 minutes are indicated. The time constants are therefore not excessively long, but care must be exercised in design so that the characteristic fluid films are of the order of 0.050 cm in thickness. Even an increase to only 1.0 mm thickness results in time constants of 2.4 and 9.2 minutes, respectively; the latter equilibration time could be unsatisfactory in many thermal control systems.

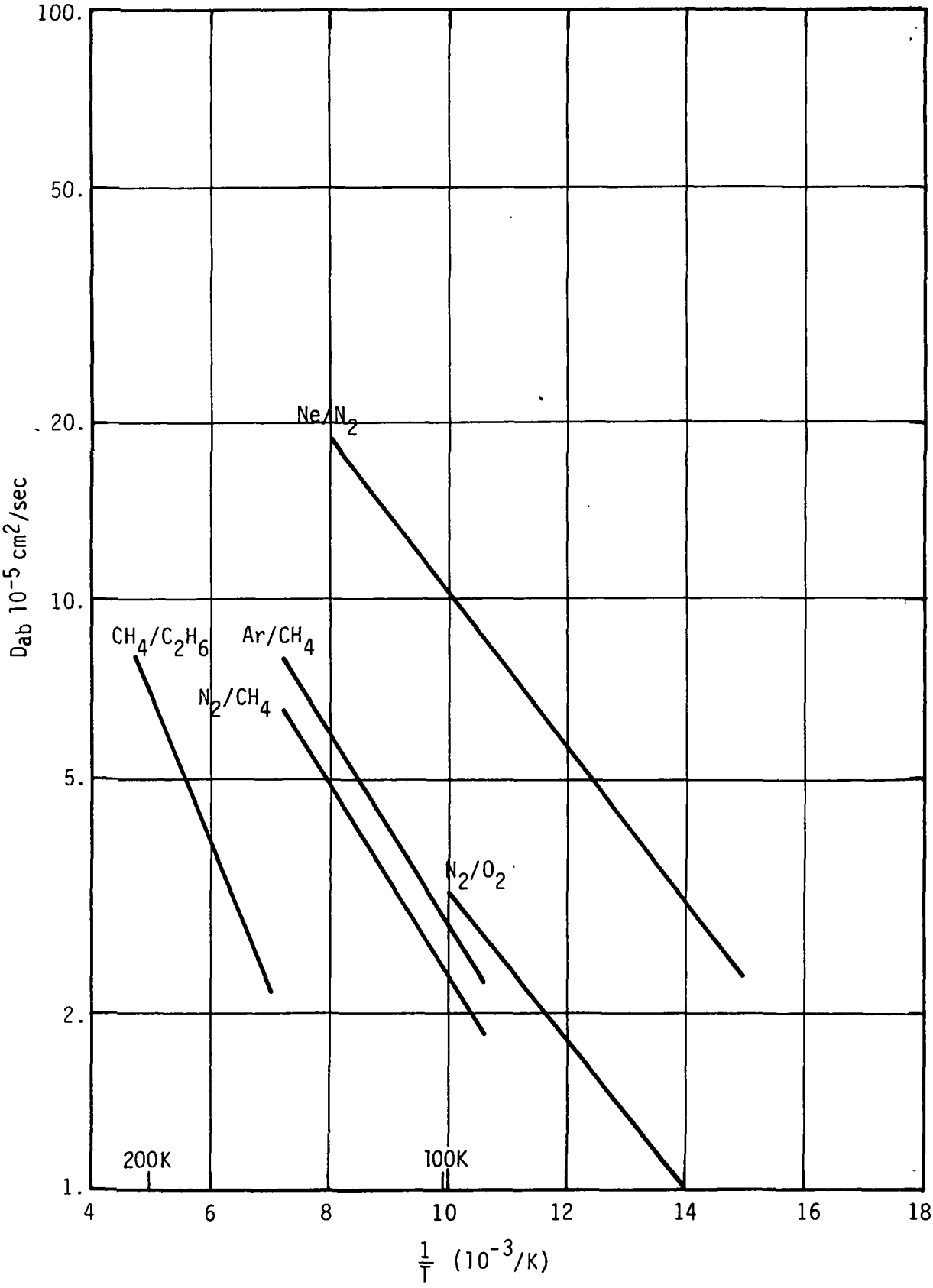

FIGURE 2.9 PREDICTED DIFFUSIVITIES FOR VARIOUS GAS-LIQUID COMBINATIONS THAT ARE OF INTEREST FOR GAS-ABSORPTION RESERVOIRS AT CRYOGENIC TEMPERATURES

TABLE 2.5. DIFFUSION TIME CONSTANTS FOR VARIOUS CRYOGENIC GAS/ LIQUID BINARY SYSTEMS (ℓ = 0.050 cm)

Gas/Liquid	Temperature (^{o}K)	Time Constant (minutes)
N_2/O_2	86.	2.3
N_2/CH_4	100.	2.0
	140.	0.7
Ar/CH_4	100.	1.6
	140.	0.6
CH_4/C_2H_6	148.	1.8
	213.	0.6

2.3.2 Coupled Heat Transfer-Diffusion Problem

Section 2.3.1 gives an order-of-magnitude model for diffusion times associated with absorption reservoir heat pipes. More precise modeling of an actual device requires coupling of heat transfer processes in the heat pipe with diffusion processes in the reservoir. This section describes analytical and numerical modeling of such a system.

2.3.2.1 Conservation of Noncondensable Gas

Unsteady-state modeling of heat pipe response requires coupled equations for conservation of energy and conservation of noncondensable gas. At time $t < 0$ the heat pipe is in equilibrium at a power level Q_1 and the total gas content N_o is given by

$$N_o = C_{gv}(0^-)\left[A_c\theta_c\ell_g(0) + V_{\ell r}\theta_r\right] \tag{17}$$

where $C_{gv}(0^-)$ denotes the gas concentration for $t < 0$, and $\ell_g(0)$ is the initial length of the gas leg. In this representation, the gas leg is assumed to end abruptly at the transition to free-flowing vapor, i.e., a 'flat front' is assumed. At $t = 0$, a step change in power level to $Q_2 > Q_1$ occurs, and conservation of noncondensable gas requires

$$N_o = C_{gv}(t)\left[A_c\theta_c\ell_g(t) + V_{\ell r}\theta_r^+\right] \tag{18}$$

where

$$\theta_r^+ = 1 + \beta_r\,(\alpha\eta_r x_r - 1) \tag{19}$$

and

$$x_r = \langle C_{g\ell}(t)\rangle / \alpha C_{gv}(t) \tag{20}$$

It is assumed that diffusion of dissolved gas into and out of the condenser wick is very rapid, and that the primary non-equilibrium condition occurs in the reservoir fluid. Deviation from equilibrium conditions at $t > 0$ is represented by x_r, which is the ratio of actual dissolved gas concentration to the dissolved concentration at the vapor-liquid interface. This interface is always assumed to be in equilibrium, that is,

$$C_{g\ell}(t) = \alpha C_{gv}(t) \qquad \text{(interface condition)} \qquad (21)$$

The average dissolved gas concentration in the reservoir is $\langle C_{g\ell}(t) \rangle$. For a slab reservoir of thickness ℓ, the average dissolved concentration is expressed as

$$\langle C_{g\ell}(t) \rangle = \alpha C_{gv}(0) + \frac{2\ D_{ab}}{\ell} \int_0^t \left(\frac{dC_{g\ell}}{dx} \right)_{x=\ell} dt \qquad (22)$$

This assumes that the slab is in vapor contact on both faces, as in Figure 2.6.

2.3.2.2 Conservation of Energy

At any instant in time, heat transferred to the heat pipe must be accounted for by heat transfer through the condenser and/or by a temperature increase of system thermal mass. For modeling ease, system thermal mass is assumed always to be in equilibrium with the vapor core temperature, $T_v(t)$. Conservation of energy at $t > 0$ results in

$$\frac{dT_v}{dt} = \frac{Q_2 - \left[G_c\left(\ell_c - \ell_g(t)\right) + G_f(\ell_g) \right] (T_v - T_s)}{mC_p} \qquad (23)$$

Heat loss via the condenser is the sum of a conductance loss from the unblocked condenser zone (ℓ_c-ℓ_g), and a conductance loss from the blocked-off zone, ℓ_g. In the latter case, the heat pipe wall in the blocked-off zone acts as an extended fin coupled to the sink with a per-unit-length conductance G_c. At the fin root, i.e., at the gas-vapor flat-front interface, the wall is assumed to be uniformly at temperature T_v. For a long condenser, where the gas zone simulates an infinitely long fin, the equivalent fin-conductance G_f is

$$G_f = \frac{\sqrt{A_w K_w G_c}}{\ell_g} \qquad \text{(W/cmK)} \qquad (24)$$

2.3.2.3 Numerical Methods

In the previous sections, the necessary conservation laws have been outlined: At any point in time, both noncondensable gas and heat input must be accounted for. However, the equations are coupled through the gas-leg length, ℓ_g, which in turn is dependent on the amount of dissolved gas in the liquid reservoir.

The various equations (18) through (23) have been solved simultaneously by numerically solving the diffusion equation in the slab reservoir wick and step-wise integrating equations (22) and (23). At each new time-step, T_v was iterated until T_v, ℓ_g, and $dC_{g\ell}/dx$ did not change by more than an arbitrary ε per iteration. When a consistent set of variables occurred, the integration in T_v proceeded to the next time-step. The trapezoidal rule was used for integrating both $dC_{g\ell}/dx$ and dT_v/dt. The iterative sequence at each time step Δt_i was

1. Calculate T_{vi} from equation (23) using previous value of ℓ_g; calculate C_{gvi}.
2. Using C_{gvi} and equation (21), calculate $dC_{g\ell}/dx\big|_{x=\ell}$ using finite differences.
3. Calculate the average dissolved gas concentration using (22).
4. Determine θ^+_{ri} from equations (19) and (20).
5. Determine a new ℓ_{gi} from equation (18).
6. Compare ℓ_{gi} with ℓ_{gi} of previous iteration. If $\Delta\ell_g < \varepsilon$, continue to next time step. If $\Delta\ell_g > \varepsilon$, go to step 1 and perform calculations using updated ℓ_{gi}.

Representative unsteady-state solutions for the time-dependent vapor core temperature $T_v(t)$ are given in Figure 3.7. These solutions are based on the experimental device detailed in Section 3.1, Experimental Methods and Apparatus.

The numerical solutions are useful in quantitatively predicting performance for a well-documented heat pipe system. However, they are also useful in establishing the relative importance of thermal time constants and diffusional time constants. That is, from equation (23) a thermal time constant can be derived

$$\tau_{th} = \frac{mC_p}{G_c\langle \ell_c - \ell_g(t)\rangle} \tag{25}$$

which is based on an average nonblocked condenser length $\langle \ell_c - \ell_g(t)\rangle$. The ratio of thermal to diffusion time constant is

$$\frac{\tau_{th}}{\tau_D} = \frac{mC_pD_{ab}}{G_c\ell^2\langle \ell_c - \ell_g(t)\rangle} = \tau^+ \tag{26}$$

The numerical solutions indicate that an overshoot in the curve $T_v(t)$ occurs for τ^+ on the order of 20. For τ^+ less than 20, the heat pipe temperature temporarily rises above the final steady-state operating temperature because of the lag in gas permeation of reservoir wicking. This criterion for τ^+ should be a valid rule-of-thumb for estimating absorption reservoir response for diverse heat pipe designs and gas/fluid selections. However, actual experimental data do not indicate an effect of diffusion limiting absorption for τ^+ much less than 20, and this divergence in behavior remains to be explored.

2.4 Analytical Summary

The temperature-control capability of a gas absorption reservoir heat pipe has been derived for both steady-state and transient conditions.

The control band of a given heat pipe design may be reduced by up to a factor of 10 by replacing a gas reservoir with an equal-volume absorption reservoir. However, absorption reservoir design requires careful consideration of mass transfer, as the dissolved gas content within the reservoir should respond rapidly to changes in heat input to reduce temperature fluctuations associated with changes in power level. Numerical models of unsteady-state behavior indicate that the ratio of heat pipe thermal time constant to diffusional time constant must be greater than or equal to approximately 20. to minimize temperature over-shoot or under-shoot when a step-change in power occurs. The temporary rise or fall in temperature of an absorption reservoir heat pipe can occur because gas diffusion in the reservoir liquid does not keep pace with the rate of temperature change based on system thermal mass.

A literature search has resulted in a number of potential gas/liquid combinations suitable for gas absorption reservoirs. Combinations have been found for both room temperature and cryogenic temperature ranges.

3.0 EXPERIMENTAL VERIFICATION

Experimental test methods are described in Section 3.1. In Section 3.2, absorption reservoir experimental results are presented, while data are correlated using models described in Section 2 in Data Interpretation, Section 3.3.

3.1 Experimental Methods and Apparatus

3.1.1 Experimental Design

Two complementary test systems have been used for experimental verification of absorption reservoir performance. Both systems use the same basic heat pipe assembly composed of evaporator, condenser, and adiabatic sections. The evaporator and condenser were each 15.24 cm long, with an adiabatic section 15.0 cm long. All three sections were 1.288 cm inside diameter. Nominal wall thickness in the condenser was 0.0650 cm, while the wall was 0.080 cm thick in the adiabatic and evaporator sections. A circumferential wall wick of 1 layer of 200 mesh square weave 304 stainless screen was used in all three sections. No bypass wick was used, and the heat pipe was operated in a slight reflux. These design and testing simplifications ensured accurate estimation of fluid volume factors without inclusion of generally uncertain correction factors for fillets. Stainless steel was used throughout. The condenser heat exchanger was anodized aluminum and was isolated from the condenser proper by an air gap of 0.022 cm for a per-unit-length gap conductance of approximately 0.0443 W/cm-K. Four 6-32 nylon adjusting screws were used at each end of the condenser block to ensure a uniform air gap. A slot in the wall of the condenser cooling block enabled direct spot-welding of the thermocouples to the condenser wall.

Two reservoir assemblies were used in testing. The first reservoir, coupled with a glass-walled section for visual observation, was formed from a spiral of 100 mesh stainless square-weave screen. This method of reservoir manufacture was found to be difficult with existing tooling and to have a low volumetric efficiency; that is, the fraction of reservoir volume filled with liquid was quite low. The glass-walled reservoir was primarily used for visual studies of fluid absorption; the experimental results presented in Section 3.2 deal exclusively with the all-metal reservoir system described below.

The metal-walled reservoir used for quantitative measurements of reservoir function is shown in Figure 3.1. In detail (A) of Figure 3.1, an axial cross section of the reservoir assembly is shown. The fluid absorption wicking was a single layer of 0.0635 cm thick felt-metal on the reservoir wall and a central cylindrical wick of 0.673 cm O.D. and 0.318 cm I.D. The central wick assembly is shown in dotted profile in (A) and in cross section in (B). The inside and outside diameters of the central wick are a single layer of 400 mesh stainless screen. The internal screened tubes, used to give the structure rigidity as well as a small priming radius, are also of 400 mesh screen and approximately 0.062 cm in diameter. Thirteen tubes were used on the inner layer and 21 tubes on the outer layer. The tubes were sealed at the end facing the condenser and maintained open at the other end to minimize bubble entrapment.

The entire reservoir is 6.81 cm long and 1.29 cm in diameter, and has a 41% volumetric fluid load. Reservoir parameters needed for modeling are given in Table 3.1.

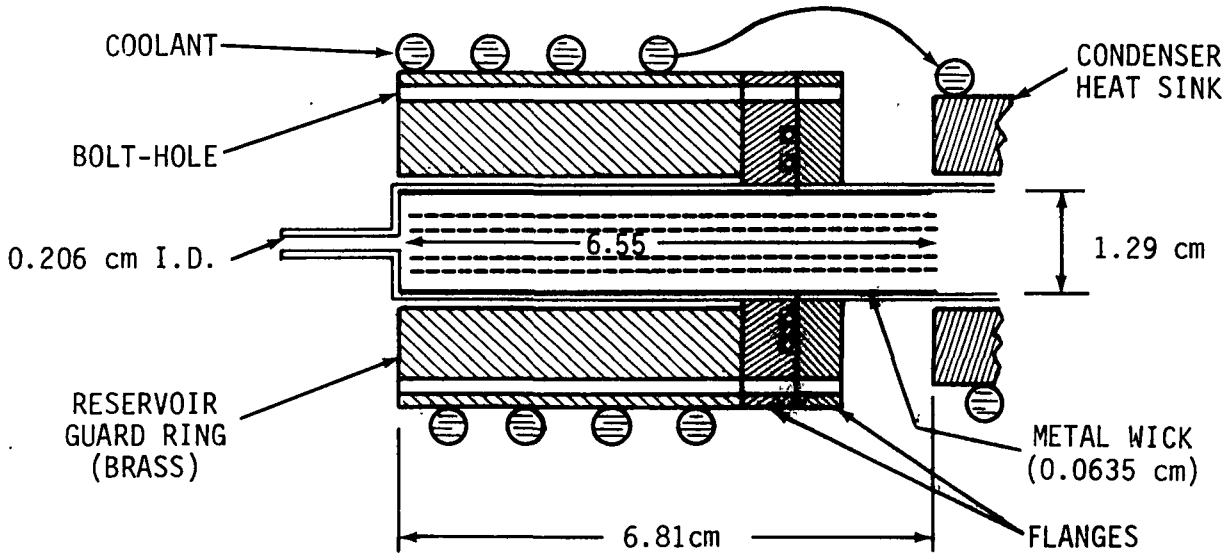

(A.) CROSS-SECTION OF RESERVOIR ASSEMBLY

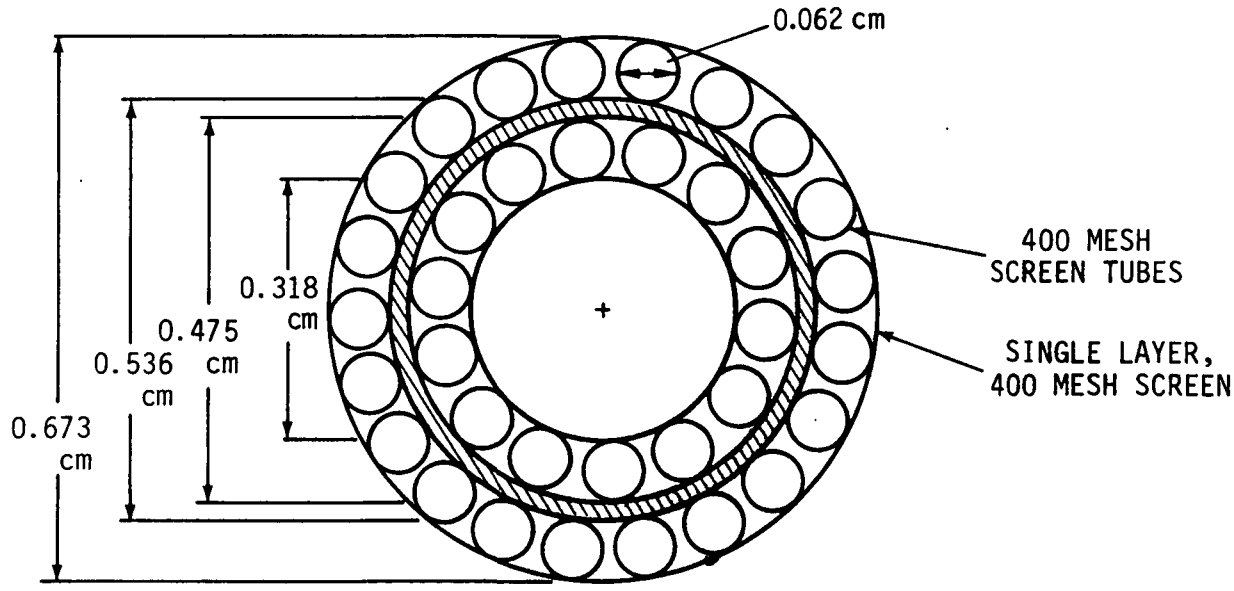

(B.) END-VIEW OF ABSORPTION RESERVOIR CENTRAL WICK

FIGURE 3.1 DETAILS OF ABSORPTION RESERVOIR DESIGN. WICK ON WALL WAS ONE LAYER OF FELT-METAL. CENTRAL RESERVOIR WICK SHOWN AS DOTTED PROFILE IN (A) IS SHOWN IN END-VIEW IN (B). WITH ALL WICKING PRIMED, 41% OF RESERVOIR VOLUME WAS FLUID-FILLED.

TABLE 3.1. RESERVOIR SPECIFICATIONS/CONDUCTANCE PARAMETERS

Reservoir total volume	8.87 cm^3
Wick/fluid volume fraction (β_r), (β_c)	0.465, 0.0375
Fluid volume fraction in wick (η_r), (η_c)	0.886, 0.68
Wick thickness	0.068 cm
Reservoir and heat sink temperature[1]	11 - 13°C
G_c	0.0443 W/cmK
Heat pipe orientation	0.24 cm favorable tilt

[1] Reservoir guard ring and condenser sink both cooled by same water circuit.

3.1.2 Testing Methods

All tests were made using methanol working fluid. The heat pipe was initially loaded with methanol and set to 0.25 cm reflux tilt to ensure an absence of fluid pooling in the condenser. Operation without noncondensable gas for several hours was used to determine leak tightness. The noncondensable gas was then inserted in sufficient quantity to allow gas control operation over the highest temperature range. Several cycles of the heat pipe from 10 to 25 watts appeared to stabilize heat pipe response, and this may be related to priming of the liquid reservoir.

After stable response was obtained, data were gathered and gas subsequently removed for heat pipe testing in a lower temperature range.

The absorption reservoir was used with the gases carbon dioxide, ammonia, and butane. After the absorption reservoir test sequence was completed, the wicking was removed from the reservoir and testing with nitrogen was used to define an experimental reference. Nitrogen has negligible solubility in methanol, in the context of this study.

An operating run was also made with all gas removed and an isothermal heat pipe to determine heat loss through the insulation package. Heat loss is linear and given as

$$Q_{\ell 1} = 0.0636\ (T_v - T_a) \quad \text{(watts)} \qquad (27)$$

where T_v is vapor temperature and T_a is ambient temperature. Heat loss via the nylon screws to the heat sink is

$$Q_{\ell 2} = 0.0226\ (T_v - T_s) \quad \text{(watts)} \qquad (28)$$

Data presented in Section 3.2 have been corrected for these two losses.

3.2 Experimental Results

Using the testing techniques given in Section 3.1.2, Figures 3.2 - 3.4 present the vapor-core heat-sink temperature difference, ΔT_{vs}, as a function of power level for the control gases N_2, CO_2, C_4H_{10}, and NH_3. As mentioned earlier, the nitrogen data were taken with the liquid reservoir wicking removed and hence represent a reference gas control design of equal reservoir volume. The temperature control band with ammonia and butane as control gases is less by about a factor of 2.5 relative to N_2 for a nominal control range of 5 to 20 watts. The experimentally determined control bands are given in Table 3.2 for the gases used. The Ostwald solubility coefficient is also given at the nominal reservoir temperature of 12.0°C.

3.3 Data Interpretation

3.3.1 Temperature Control

Table 3.2 presents a comparison of experimental and predicted performance for both the absorption reservoir tests with CO_2, C_4H_{10} and NH_3 and gas reservoir tests with nitrogen. In general, the gases C_4H_{10} and NH_3 had, for a given heat transfer band-width, a temperature band-width 1/2 to 1/3 that seen with the standard gas reservoir and nitrogen. This difference amounts to a saving in reservoir volume of a factor of 5 to 7.5.

The data comparison in Table 3.2 is based on $\Delta T/\Delta Q$. The heat pipe vapor core temperature was found to be essentially linearly dependent on Q, the heat transfer rate, provided that the gas front resided in the condenser. Therefore, the control capability has been characterized on the basis of the slope of the function $T_v(Q)$. In each test, the slope $\Delta T/\Delta Q$ was calculated by a least-squares fit to the data over the linear region. The data have also

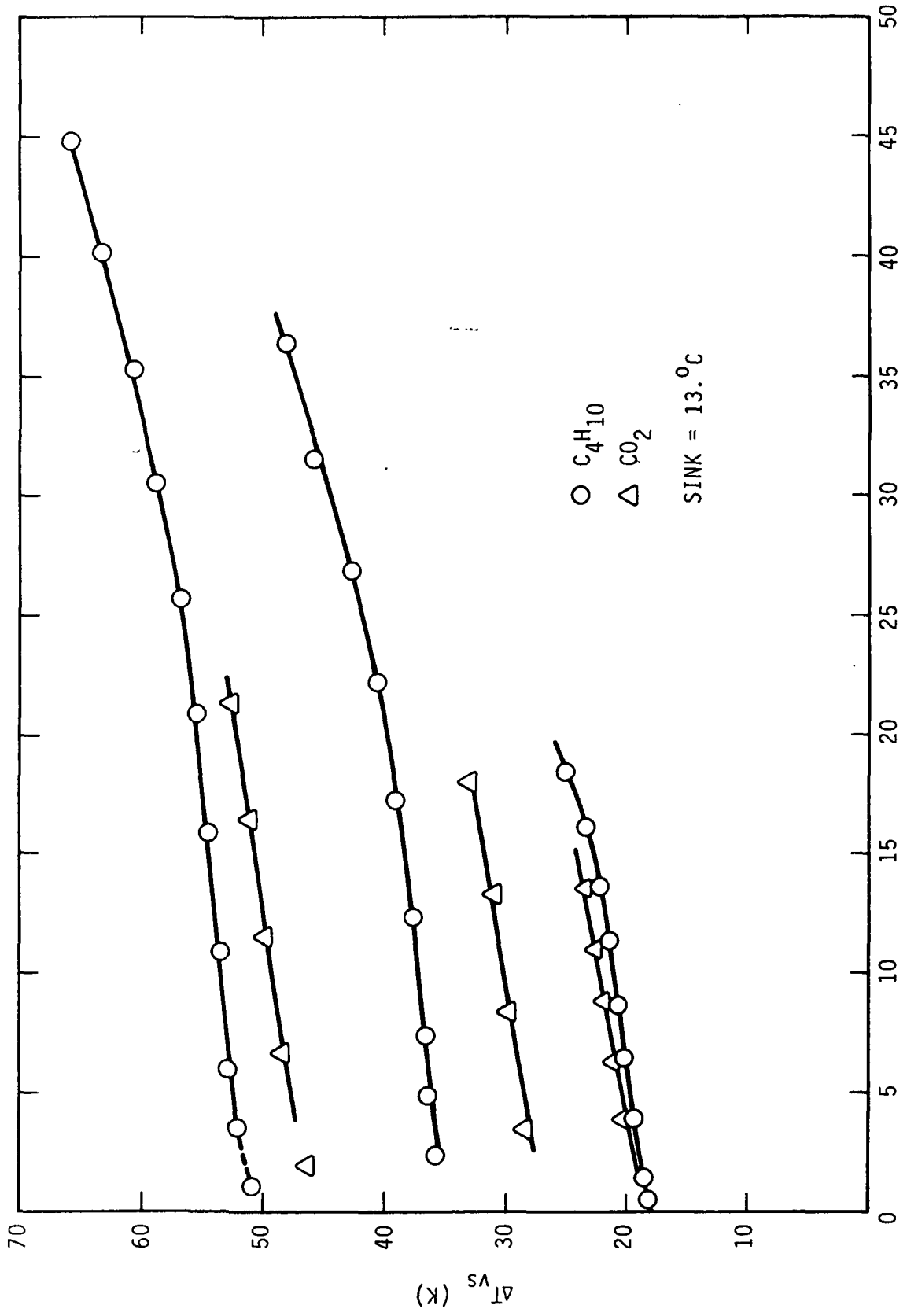

FIGURE 3.2 TEMPERATURE DIFFERENCE BETWEEN HEAT PIPE VAPOR CORE AND CONDENSER HEAT SINK FOR THE CONTROL GASES n-C_4H_{10} AND CO_2. DATA TAKEN WITH ABSORPTION RESERVOIR.

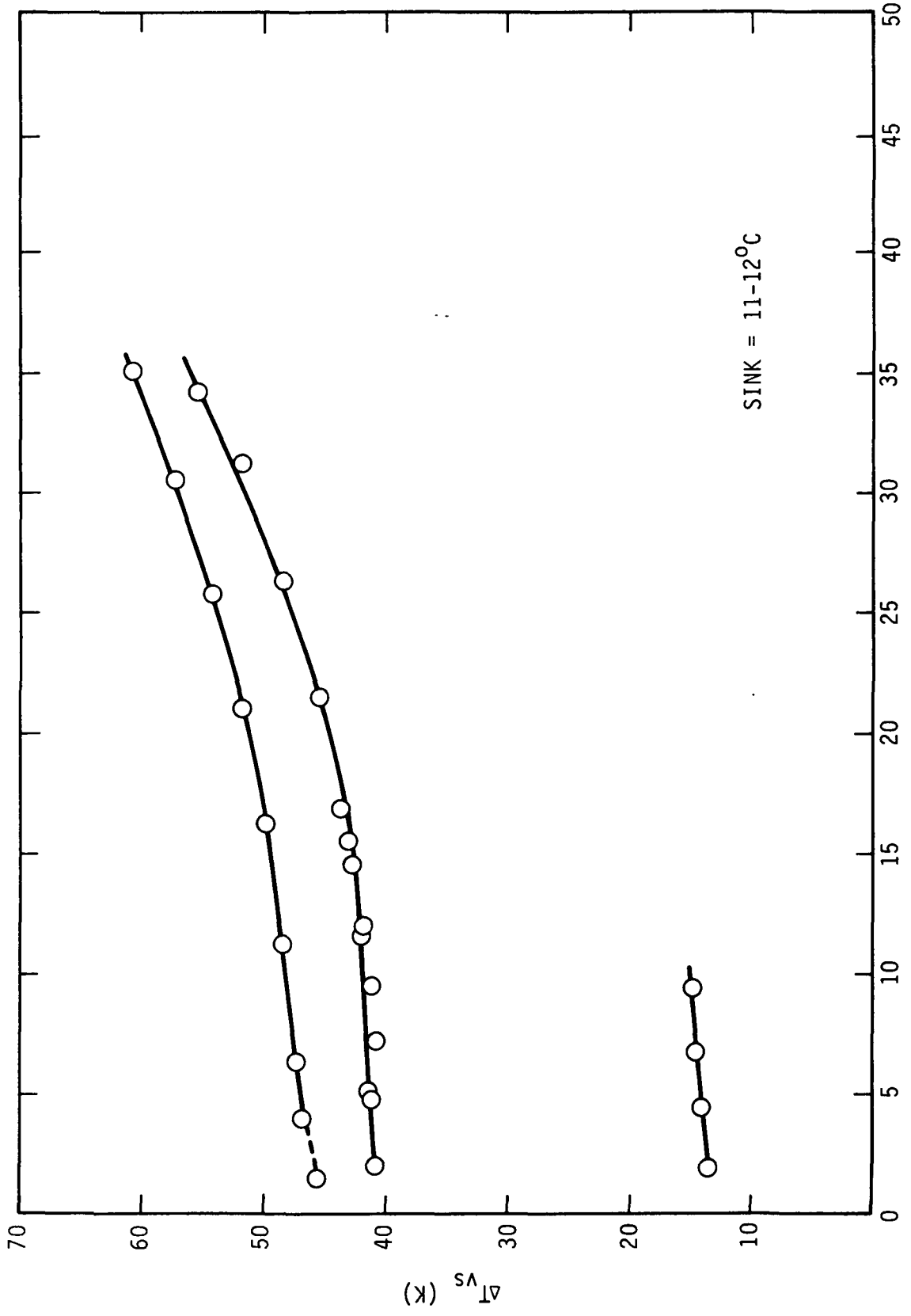

FIGURE 3.3 TEMPERATURE DIFFERENCE BETWEEN HEAT PIPE VAPOR CORE AND CONDENSER HEAT SINK FOR AMMONIA CONTROL GAS. DATA TAKEN WITH ABSORPTION RESERVOIR

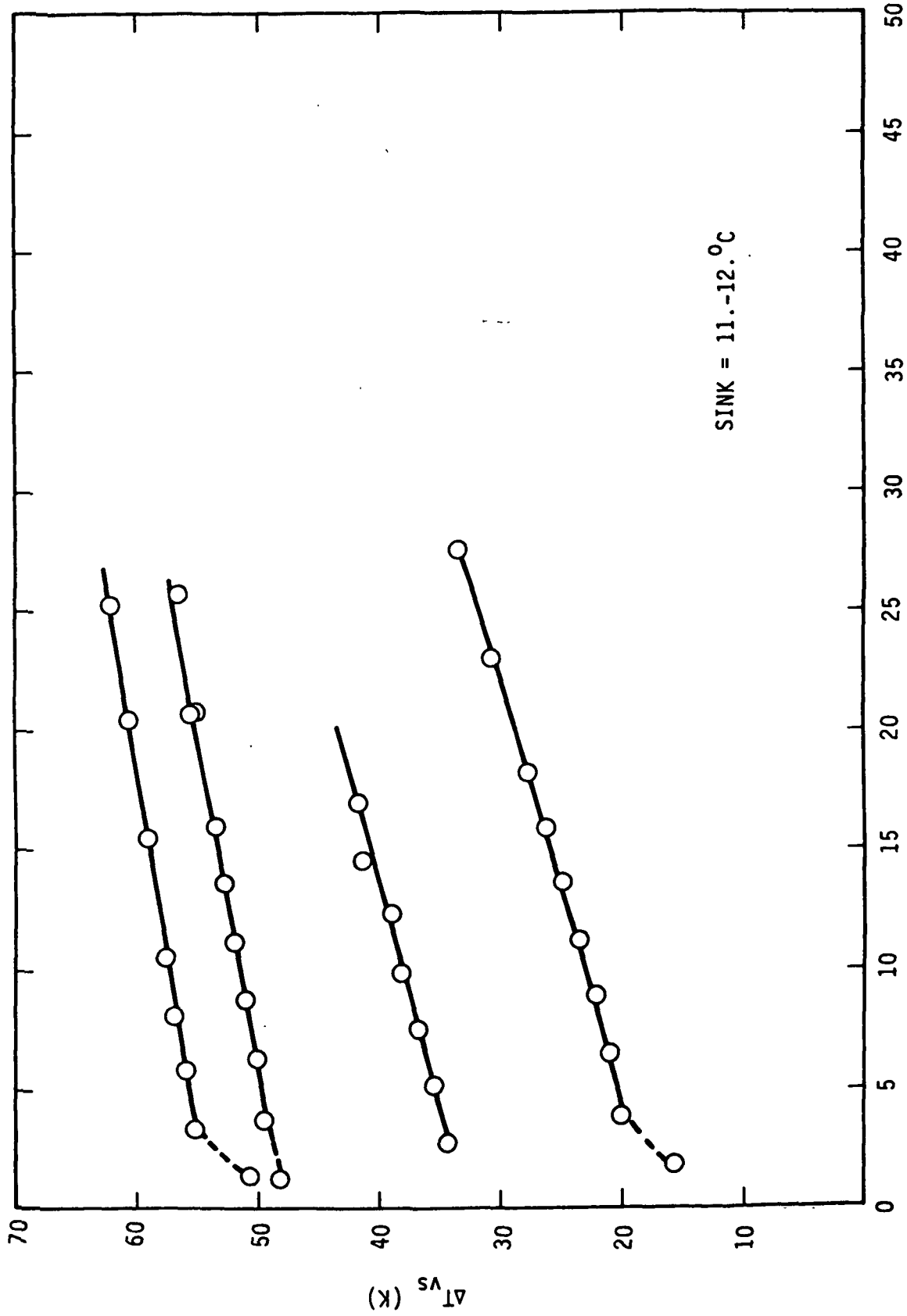

FIGURE 3.4 TEMPERATURE DIFFERENCE BETWEEN HEAT PIPE VAPOR CORE AND CONDENSER HEAT SINK FOR NITROGEN CONTROL GAS. THIS DATA HAS BEEN TAKEN WITH THE ABSORPTION WICKING REMOVED; THE RESERVOIR IS FUNCTIONING AS A STANDARD GAS RESERVOIR.

TABLE 3.2. EXPERIMENTAL DATA SUMMARY FOR VARIOUS GAS CONTROL TESTS WITH METHANOL WORKING FLUID AND A RESERVOIR TEMPERATURE OF 11 to 13°C

Control Gas	Reservoir[1]	ΔT/ΔQ (K/W)	Average Value of ΔT/ΔQ	Ostwald Coefficient	Estimated Value of ΔT/ΔQ[2]	Percent Deviation Data From Theory
Nitrogen	S	0.545, 0.535, 0.358	0.48±0.11	0.125	0.49-0.73	-20
Carbon Dioxide	A	0.396, 0.319 0.296	0.34±0.05	4.1	0.37-0.53	-24
Butane	A	0.301, 0.235, 0.197	0.24±0.05	~28.	0.17-0.24	+14
Ammonia	A	0.191, 0.161, 0.256	0.20±0.05	~220.	0.097-0.11	+100

(1) S = standard design, wetted reservoir
A = Absorption Reservoir

(2) Based on a flat gas-vapor interface

been organized by the nominal vapor-sink operating temperature difference in the range 7.5 to 10.0 watts. The resulting data ranges, and the lengths of the linear regions are approximately as follows

Region 1: ΔT_{vs} @ 8.75 w = 22.5°C; linear span = 2.0 to 12.5 W

Region 2: ΔT_{vs} @ 8.75 w = 37.5°C; linear span = 2.5 to 15.0 W

Region 3: ΔT_{vs} @ 8.75 w = 50.0°C; linear span = 4.0 to 17.5 W

The experimental values of $\Delta T/\Delta Q$ in Table 3.2 represent each temperature region investigated. For comparison with calculated values of $\Delta T/\Delta Q$, the individual values have been averaged. Both the averaged and individual experimental values are presented in Figure 3.5 for relative comparison.

Control capability of the absorption reservoir is in qualitative agreement with estimated values of $\Delta T/\Delta Q$ using a flat-front model and the dissolution models discussed in Section 2. The experimental control ratios compare with theory as follows

$\Delta T/\Delta Q$ for N_2;	20% lower than theory
CO_2;	24% lower than theory
C_4H_{10};	14% higher than theory
NH_3;	100% higher than theory

The general experimental trend is a reduced effect of Ostwald coefficient although performance improvements are still apparent as α increases. Figure 3.6 shows the experimental data compared to predicted control ratios for an Ostwald coefficient range from 1.0 to 1000.

The reduced influence of α beyond about 30 may be attributable to a spreading out of the gas front because of high solubility. Condenser thermocouples indicated a considerably longer gas front with the three soluble gases than with nitrogen. However, because of differences in molecular

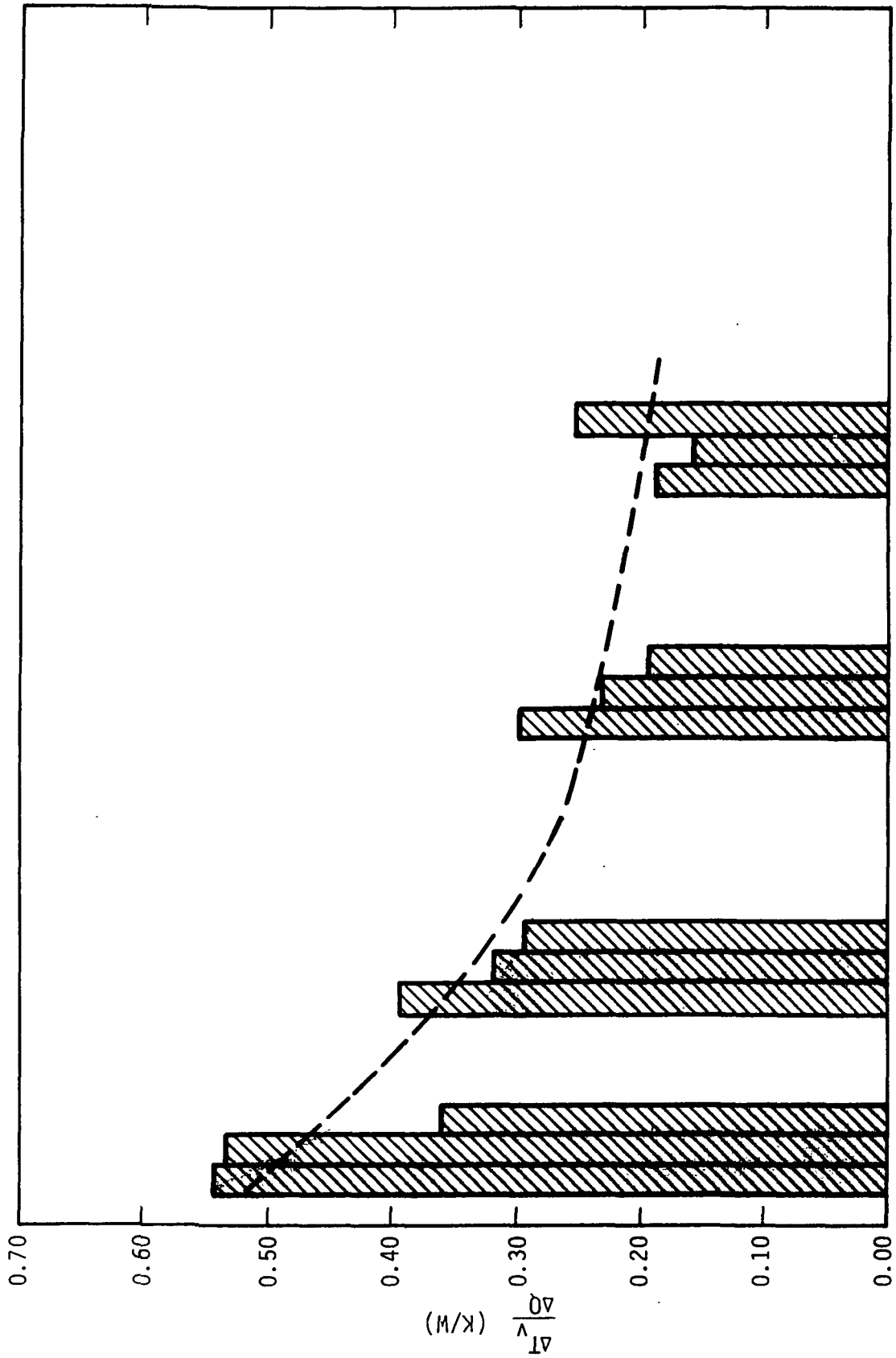

FIGURE 3.5 A GRAPHICAL ILLUSTRATION OF THE EXPERIMENTALLY DETERMINED EFFECT OF CONTROL GAS SPECIES ON CONTROL RATIO. THE THREE GASES, CO2, C4H10, AND NH3 WERE USED WITH THE RESERVOIR 41% FILLED WITH FLUID. THE NITROGEN TEST WAS WITH ALL WICKING REMOVED FROM THE RESERVOIR, AND IT HENCE SERVES AS A REFERENCE GAS RESERVOIR DESIGN. TEMPERATURE VARIATION WITH HEAT INPUT FLUCTUATION WAS REDUCED BY A FACTOR OF ABOUT 2.5.

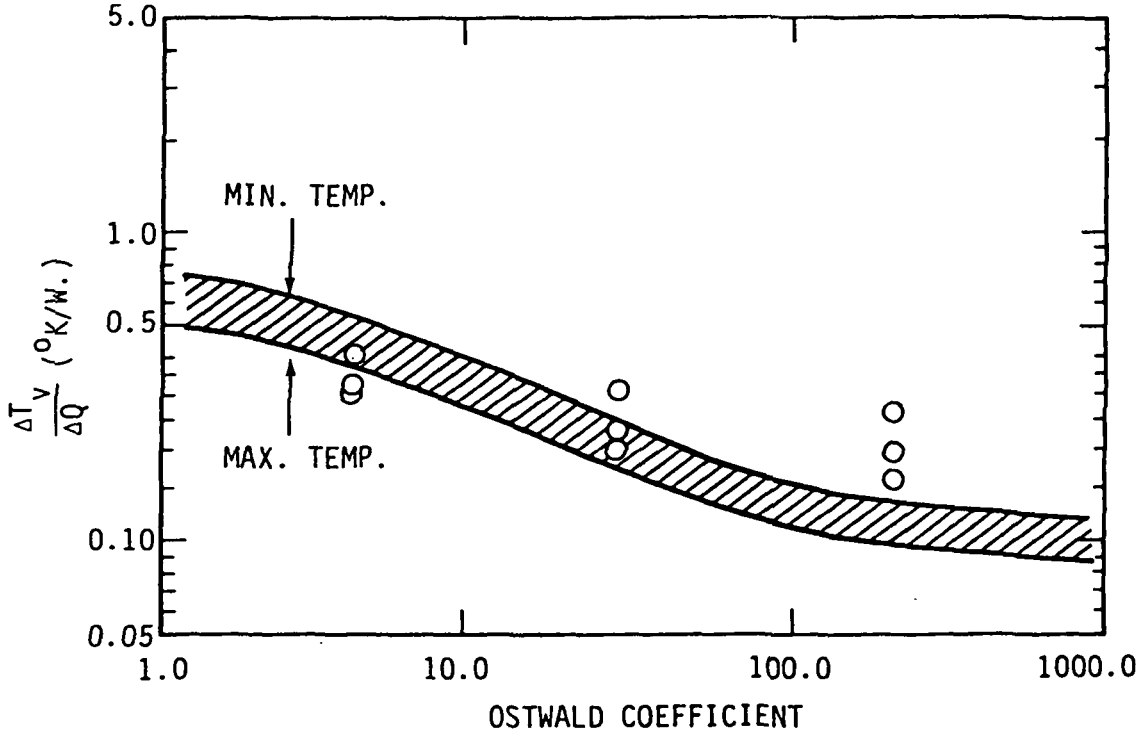

FIGURE 3.6 RATE-OF-CHANGE OF VAPOR CORE TEMPERATURE WITH RESPECT TO HEAT INPUT FOR THE THREE SOLUBLE CONTROL GASES USED WITH METHANOL WORKING FLUID. THE THEORETICAL INFLUENCE OF SOLUBILITY ON TEMPERATURE CONTROL IS ALSO SHOWN, ASSUMING A SHARP GAS-VAPOR INTERFACE. THE BAND STRUCTURE REFLECTS MAX. OPERATING TEMPERATURE RANGE.

weight between the gases and working fluid vapor, vertical gravity-force stratification of the gas front could produce the same broadening. Another possibility is that small amounts of insoluble gas either leak into the heat pipe via O-rings or hydrogen is generated from water contained in the methanol. The direct effect of this will be a reduction in control ratio which becomes increasingly important as α increases in size. Further investigation of this effect is warranted.

In summary, the temperature change resulting from a given heat input change has been reduced by a factor of two to three for an absorption reservoir of identical volume to a gas reservoir. This has been demonstrated with a common gas-control heat pipe working fluid, methanol. Equivalent performance with a wetted wall gas reservoir would require a volumetric increase to about 5x to 7.5x the volume of the absorption reservoir.

3.3.2 Transient Response

Figure 3.7 presents experimental data on time response of vapor core temperature to a step-increase in heat transfer rate from approximately 5 watts to 20 watts at a nominal vapor temperature of 55^{o}C above sink temperature. The vapor core temperature is nondimensionalized by defining

$$\frac{\Delta T_v}{\Delta T_{vm}} = \frac{T_v(t) - T_{vo}}{T_{vm} - T_{vo}} \tag{29}$$

where T_{vo} is the initial vapor temperature and T_{vm} is the final vapor temperature. The experimental data do not show any significant effect of reservoir design or control gas on transient response. However, various amounts of over-shoot are analytically predicted for the absorption reservoir system depending on the diffusion coefficient of the gas in the working fluid. The

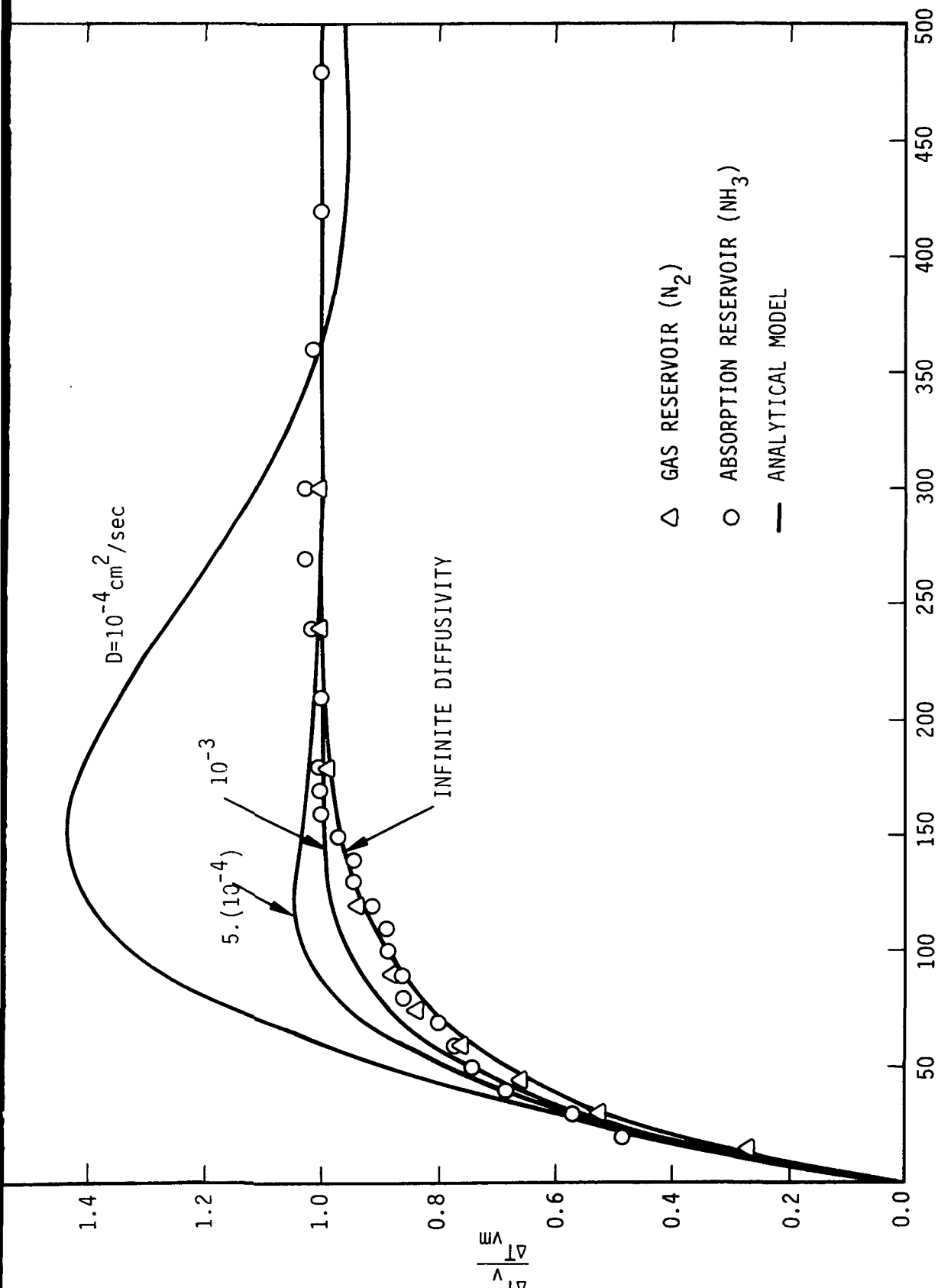

FIGURE 3.7 TRANSIENT RESPONSE OF THE ABSORPTION RESERVOIR HEAT PIPE TO A STEP-INCREASE IN HEAT INPUT. RESPONSE OF THE REFERENCE GAS RESERVOIR (i.e., N_2 GAS WITH THE WICK REMOVED FROM 5 W to 20 W ABSORPTION RESERVOIR) IS ALSO SHOWN FOR COMPARISON. ANALYTICAL MODELS FOR TRANSIENT RESPONSE PREDICT MUCH LARGER TRANSIENTS THAN WERE ACTUALLY MEASURED, INDICATING VERY LARGE EFFECTIVE GAS/LIQUID DIFFUSIVITIES.

diffusivity of ammonia gas in methanol is estimated to be 5 to 10 (10^{-5}) cm^2/sec. For this range of diffusivity, about a 40% over-shoot in dimensionless temperature is predicted, while only a few percent was observed. Butane gas also displayed minimal over-shoot and under-shoot.

Alternate explanations for this divergence in behavior remain to be explored. It is possible that the high solubility of these gases in methanol creates a turbulent mass transfer phenomena that is much more effective than simple diffusion. However, if this is correct, then it must be determined if these turbulent transfer processes will function in zero-g, since they could require a gravity field.

An alternate explanation is that the diffuse gas front found for soluble gas/liquid combinations is a function of both radial and axial position, so that the absorption process and overall heat transfer coefficient are not adequately described by a flat-front gas control model. Vertical stratification of the gas front could also create experimental deviation from analytical predictions.

Viability of the absorption reservoir technique has been demonstrated on the basis of heat transfer. However, questions raised related to transient response and gravity effects should be explored in further detail to fully substantiate performance of the reservoir in a zero-g environment.

4.0 CONCLUSIONS

Significant improvements in thermal control have been experimentally demonstrated for the absorption reservoir. With the same volume as a reference gas reservoir, temperature control has been improved by a factor of two to three for butane and ammonia control gases with methanol working fluid. A smaller improvement was shown for carbon dioxide, a gas with lower solubility in methanol. Equivalent thermal performance from a gas reservoir would require a volume 5 to 7.5 times that used with the absorption reservoir and ammonia or butane. Detailed comparisons of absorption reservoir tests, standard reservoir tests with equal volume, and theoretical predictions are given in Table 3.2. Transient response was relatively unaffected by reservoir design, and heat pipe response to a step-change in heat transfer rate was very rapid.

However, this responsiveness is very interesting in that the experimental heat pipe was expected to exhibit a relatively large transient temperature over-shoot on the basis of diffusion rate constants for the liquid absorption reservoir. Further analytical and experimental work is needed to determine the basis for this unexpected performance improvement, since the apparent improvement in mass transfer may be related to gravity-assisted convection effects not present in zero-g.

In addition, temperature measurements on the outside of the condenser indicated a very diffuse gas front in the case of the soluble gases ammonia, butane, and carbon dioxide. The gas front was relatively sharp in the case of nitrogen, which is relatively insoluble in methanol and very close in molecular weight. A diffuse gas front and/or a front that is vertically stratified because of gravity effects may partially account for the improved

gas control, independent of the soluble gas reservoir effect; the thermal effects of nonperpendicular gas fronts are not well understood. It would be of interest to redesign the test apparatus so that the heat pipe could be operated in a vertical reflux position with a lower molecular weight gas such as ammonia. In a vertical position, the ammonia-methanol vapor phase mixture would effectively float on the lower density methanol vapor below.

By carefully comparing operating characteristics in both horizontal and vertical modes, the effects of gravity on gas front shape could be determined, and transient response behavior linked to either a gas-front related-mechanism or reservoir mass transfer mechanism.

REFERENCES

1. E. W. Saaski, Condensation Heat Transfer in a Closed Tube Containing a Soluble, Noncondensable Gas, NASA Final Report CR 137811, December 1975.

2. E. W. Saaski, Investigation of Bubbles in Arterial Heat Pipes, NASA CR 114 531, December 1972.

3. E. Thomsen and J. Gjaldbaek, Acta Chemica Scandannavica, Vol 17, 134 (1963).

4. W. Bowden, et al., J. Chem. Eng. Data, Vol. 11, No. 3, 296 (1966).

5. W. Hayduk and H. Laudie, AICHE J., Vol. 19, No. 6, 1233 (1973).

6. M. Iino, et al., J. Chem. Eng. Data, Vol. 15, No. 3, 446 (1970).

7. J. Chu, et al., Vapor-Liquid Equilibrium Data, J. W. Edwards Publ., Ann Arbor, Michigan, 1956.

8. L. O. Roellig and C. Geise, J. of Chem. Phys., Vol. 37, No. 1, 114 (1962).

9. F. E. Karasz and G. D. Halsey, Jr., J. of Chem. Phys., Vo. 29, No. 1, 173 (1958).

10. E. Sinor and F. Kurata, J. of Ch. Eng. Data, Vol. 11, No. 4, 537 (1966).

11. R. J. Burch, J. of Ch. Eng. Data, Vol. 9, No. 1, 19 (1964).

12. A. L. Benham and D. L. Katz, AICHE J., Vol. 3, No. 1, 33 (1957).

13. R. E. Latimer, AICHE J., Vol. 3, No. 1, 75 (1957).

14. G. Armstrong, et al., J. Res. N.B.S., Vol. 55, No. 5, 265 (1955).

15. H. Cheung and D. Wang, I and EC Fund., Vol. e, No. 4, 355 (1964).

16. F. B. Sprow and J. M. Prausnitz, Cryogenics, December 1966, p. 338.

17. F. P. Ricci, Diffusion in Simple Liquids, Phys. Rev., Vol. 156, No. 1, 184, 1967.

APPENDIX A

Diffusion From a Double-sided Slab

Given the physical system shown in Figure 2.6, it is desired to solve the diffusion equation in one dimension

$$\frac{\partial C}{\partial t} = D_{ab} \frac{\partial^2 C}{\partial x^2} \tag{1}$$

A dimensionless distance and concentration are defined as

$$x^* = \pi x/\ell \tag{2}$$

$$C^* = (C-C_o)/(C_m-C_o) \tag{3}$$

Boundary conditions are assumed to be

@ $t=0$, $C^*=1$ for all x^*

@ $t=0^+$, $C^*=0$ for $x^*=0$ and $x^*=\pi$

for $t \to \infty$, $C^*=0$ for all x^*

The diffusion equation now becomes

$$\frac{\partial C^*}{\partial t} = D^* \frac{\partial^2 C^*}{\partial x^{*2}} \tag{4}$$

where

$$D^* = \left(\frac{\pi}{\ell}\right)^2 D_{ab}$$

This has the Fourier sine series solution

$$C^* = \sum_{N=1}^{\infty} b_N \, \mathrm{EXP}(-N^2 D^* t) \sin(Nx^*) \tag{5}$$

where

$$b_N = \frac{2}{\pi} \int_0^{\pi} C^*(t=0) \sin(Nx^*) dx^* \tag{6}$$

Using the initial concentration distribution, the solution (5) is alternatively given as

$$C^* = \frac{4}{\pi} \sum_{N=1}^{\infty} \frac{\text{EXP}(-(2N-1)^2 D^* t) \sin (2N-1)x^*}{2N-1} \tag{7}$$

If expression (7) is integrated in x^* and divided by the interval length, then the average concentration is found to be

$$\bar{C}^* = \frac{8}{\pi^2} \sum_{N=0}^{\infty} \frac{\text{EXP}\,[-(2N+1)^2 D^* t]}{(2N+1)^2} \tag{8}$$

~~29 SEP 76~~ ~~R. V. Mask E242/106~~ 3/27458

22 NOV 76 R. G. Nagle E242/106/L 66 m/

MAR 1992

Turn inside

SIGMA RESEARCH, INC.
2952 GEORGE WASHINGTON WAY
RICHLAND, WASHINGTON 99352

RESEARCH, DEVELOPMENT, DESIGN, ANALYSIS AND PLANNING, PHYSICS, BIOLOGY, AND MECHANICAL, CHEMICAL, AND OPTICAL ENGINEERIN